

Investigation into the Third Order Nonlinear Optical Properties of Potential Harmonophores

By Elisha Marie Bennett

A Thesis Submitted to

Saint Mary's University, Halifax, Nova Scotia

In Partial Fulfilment of the Requirements for the Degree of Bachelor of Science with Honours in
Chemistry

March 2023, Halifax, Nova Scotia

Copyright Elisha Marie Bennett, 2023

Supervisor: Dr. Danielle Tokarz

Department Chair: Dr. Jason Masuda

Date: April 26, 2023

Certification

Investigation into the Third Order Nonlinear Optical Properties of Potential Harmonophores

By: Elisha Marie Bennett

Copyright Elisha Marie Bennett, 2023

I hereby certify that this thesis was completed by Elisha Marie Bennett in partial fulfillment of the requirements of the Degree of Bachelor of Science with Honours in Chemistry at Saint Mary's University and I certify that this is truly original work carried out by Elisha Marie Bennett.

Thesis Supervisor

Chairperson of the Chemistry Department

Date: April 26, 2023

Abstract

Investigation into the Third Order Nonlinear Optical Properties of Potential Harmonophores

By Elisha Marie Bennett

Third harmonic generation (THG) microscopy uses the nonlinear optical effect called harmonic generation (HG) to study materials and compounds. It is an advantageous technique for biological imaging, as unlike fluorescence microscopy, it does not risk damaging the sample through photobleaching. In this, imaging is performed by contrasting the difference in the THG signal generated by the sample. This difference can be enhanced for the sample through the use of dyes that act as strong harmonophores, which are compounds that generate strong THG signal. The ability to generate strong THG signal can be evaluated through determining the second hyperpolarizability (γ) value for the compound.

In this thesis, an investigation into the nonlinear optical properties of starting materials and a set of pyrrole compounds for a series of ruthenium-pyrrole complexes was performed using THG microscopy. The second hyperpolarizability (γ) values for each compound were determined using the THG ratio technique. This work acts as a base to evaluate how to optimize the ruthenium-pyrrole complexes to improve their potential for use as dyes for THG microscopy.

April 26, 2023

Acknowledgements

First, I would like to thank Dr. Danielle Tokarz and Dr. Richard Cisek for the opportunity to do my honours and work in research over the past few years. I would also like to thank them for their guidance and support during the course of this project. I would also like to thank all current and past Tokarz lab group members: Macaulay Harvey, Hwanhee Jeon, Ryan Holmes, Margaret MacLellan, Selina Jan Gaudreault, and Sasha MacArthur.

I would also like to thank Dr. Najwan Albarghouthi, Dr. Bitu Hurisso, Dr. Elizabeth McLeod, and the rest of the chemistry department, as well as Dr. Alison Thompson and her research group for supplying the compounds for my project.

Lastly, I would also like to thank my family and friends for their continued support, especially my mom, Allison Bennett, and my partner Jacob Hoare for his love and encouragement throughout my degree.

Table of Contents	Page #
Abstract	iii
Acknowledgements	iv
List of Figures	vii
List of Schemes	x
List of Tables	xi
List of Equations	xii
List of Abbreviations	xiii
Chapter 1: INTRODUCTION.....	1
1.1 Research Overview	1
1.2 Objectives of Thesis	1
CHAPTER 2: BACKGROUND.....	3
2.1 Theory	3
2.1.1 Harmonic Generation Microscopy	3
2.1.2 Second Harmonic Generation Microscopy.....	5
2.1.3 Third Harmonic Generation Microscopy	8
2.1.4 Refractive Index	12
2.2 Literature Review	13
2.2.1 Introduction	13
2.2.2 Non-biological Harmonophores in THG Microscopy	14
2.2.3 Computational Studies on Potential Harmonophores.....	17
2.2.4 Biological Compound Based Harmonophores in THG Microscopy	19
Chapter 3: EXPERIMENTAL	22
3.1 Materials.....	22

3.2 Experimental Determination of γ Values	22
3.2.1 Solution Preparation	22
3.2.2 Refractive Index Measurements	23
3.2.3 THG Intensity Ratio Measurements	24
Chapter 4: RESULTS AND DISCUSSION	27
4.1 Salt Solutions	27
4.2 Starting Material Core Compounds.....	30
4.2.1 Benzene Ring Cores	30
4.2.2 Naphthalene Cores.....	34
4.2.3 4,7-dibromobenzo[c]-1,2,5-thiadiazole	39
4.3 Pyrrole Compounds for Potential Dye Complexes	41
4.3.3 2-(2-phenylethenyl)-1H-pyrrole (AAA40).....	41
4.3.4 5-(2-Phenylethenyl)-1H-pyrrole-2-carboxaldehyde (AAA41).....	42
Chapter 5: CONCLUSION	44
Chapter 6: FUTURE WORK	46
CHAPTER 7: REFERENCES	47
CHAPTER 8: APPENDIX	53

List of Figures

Figure 1. A pictorial representation of harmonic generation. ⁶ SHG is depicted in the on the left, in which two photons combine to form a photon with twice the frequency (2ω). ⁶ In the center, THG is depicted in which three photons combine to form a photon with three times the frequency (3ω). ⁶ Higher harmonic generation (HHG) is represented on the right with the number of photons being represented by n, where n is greater than 3.....	3
Figure 2. Combination of two photons with a given frequency when interacting with a noncentrosymmetric material to form a photon with twice the frequency of the excitation beam. 6	
Figure 3. A comparison of fluorescence (Fl) and THG. Fl involves the absorption of a photon with a given frequency (ω), a Stokes shift of the excited electron (orange arrow), and emission of a lower energy photon (F). THG involves the combination of three photons with a given frequency (ω) to generate a photon with three times the frequency (3ω). This process does not occur at the excited state but rather at a virtual state.....	8
Figure 4. Depiction of the Gouy phase shift (a) where the THG signal produced on either side is cancelled out due to a phase shift in π radians. The breaking of the focal volume symmetry (b) is represented by the arrows coming from the rectangle around the compound of interest. The rectangle represents an interface between a sample and a surrounding material.	10
Figure 5. The molecular structure for the dicyanovinylbenzene compounds, where R = -H, -Cl, -OH, -N(CH ₃) ₂ . ⁹	15
Figure 6. The molecular structure for the tetrathiafulvalene-appended azine ligands, where R = -NO ₂ , CH ₃ . ²³	16
Figure 7. The molecular structure for 7-amino-2-p-tolyl-2H-thiazolo[3,2-a]pyrimidine-3,5-dione (a) and (E)-methyl 2-amino-4,5-dihydro-4-p-tolylpyrido[3,2-b][1,4]oxazepine-3-carboxylate (b). ³⁶	18
Figure 8. The molecular structure of β -carotene. ⁸	19
Figure 9. Labelled image of the home-built UV to near IR tunable refractometer.....	24
Figure 10. Schematic of homebuilt nonlinear optical THG microscope with pictorial representation of the different interfaces. Abbreviations: SM (Scanning Mirrors), LP (Linear Polarizer), HWF (Half-Wave Plate), AO (0.3 NA Air Immersion Objective), CO (0.85 NA Collection Objective), F (Filter), PMT (Photomultiplier Tube Detector)	25

Figure 11. The refractive indices and THG intensity ratios used in the determination of the second hyperpolarizability value for NaCl. The refractive indices taken at 343 nm (THG) and 1030 nm (IR) (a), the THG intensity ratios (b), and the third order nonlinear susceptibility values (c) plotted over the concentration of the NaCl solutions. Errors bars are given for each graph.	27
Figure 12. The refractive indices taken at 343 nm (THG) and 1030 nm (IR) (a), the THG intensity ratios (b), and the third order nonlinear susceptibility values (c) plotted over the concentration of the MgSO ₄ solutions.	28
Figure 13. The solvent shell for magnesium and sulfate ions in water in the SIP and CIP structure. ³⁸	29
Figure 14. The refractive indices and THG intensity ratios used in the determination of the second hyperpolarizability value for bromobenzene and 1,4-dibromobenzene. The refractive indices taken at 343 nm (THG) and 1030 nm (IR) for bromobenzene (a) and 1,4-dibromobenzene (d), the THG intensity ratios for bromobenzene (b) and 1,4-dibromobenzene (e), and the third order nonlinear susceptibility values plotted over the concentration of the diluted bromobenzene solutions (c) and 1,4-dibromobenzene solutions (f).	31
Figure 15. The refractive indices and THG intensity ratios used in the determination of the second hyperpolarizability value for naphthalene. The refractive indices taken at 343 nm (THG) and 1030 nm (IR) (a), the THG intensity ratios (b), and the third order nonlinear susceptibility values (c) plotted over the concentration of the naphthalene solutions.....	34
Figure 16. The refractive indices and THG intensity ratios used in the determination of the second hyperpolarizability value for 2-bromonaphthalene and 2,6-dibromonaphthalene. The refractive indices taken at 343 nm (THG) and 1030 nm (IR) 2-bromonaphthalene (a) and 2,6-dibromonaphthalene (d), the THG intensity ratios 2-bromonaphthalene (b) and 2,6-dibromonaphthalene (e), and the third order nonlinear susceptibility values plotted over the concentration of the 2-bromonaphthalene solutions (c) and 2,6-dibromonaphthalene solutions (f).	35
Figure 17. Pictorial representation of naphthalene (a) and 2,6-dibromonaphthalene (b) molecular structures. The MEP for naphthalene (c) (Reproduced with permission from Spectrochimica acta part A: molecular and biomolecule spectroscopy, Elsevier) ⁴⁴ and 2,6-dibromonaphthalene (d) (Reproduced with permission from Journal of molecular structure, Elsevier) ⁴³ . Red regions are negatively charged whereas blue regions are positively charged.	39

Figure 18. The refractive indices and THG intensity ratios used in the determination of the second hyperpolarizability value for DBTD. The refractive indices taken at 343 nm (THG) and 1030 nm (IR) (a), the THG intensity ratios (b), and the third order nonlinear susceptibility values (c) plotted over the concentration of the DBTD diluted solutions. 40

Figure 19. The refractive indices and THG intensity ratios used in the determination of the second hyperpolarizability value for AAA40. The refractive indices taken at 343 nm (THG) and 1030 nm (IR) (a), the THG intensity ratios (b), and the third order nonlinear susceptibility values (c) plotted over the concentration of the AAA40 diluted solutions. 41

Figure 20. The refractive indices and THG intensity ratios used in the determination of the second hyperpolarizability value for AAA41. The refractive indices taken at 343 nm (THG) and 1030 nm (IR) (a), the THG intensity ratios (b), and the third order nonlinear susceptibility values (c) plotted over the concentration of the AAA41. 42

List of Schemes

Scheme 1	29
----------------	----

List of Tables

Table 1. The bromobenzene based ruthenium complex series. This acts as a representative example for each of the starting materials evaluated in this work.....	2
Table 2. The structure and name of the compound and its experimental γ value.	33

List of Equations

Equation (1)	4
Equation (2)	4
Equation (3)	4
Equation (4)	6
Equation (5)	6
Equation (6)	11
Equation (7)	11
Equation (8)	12
Equation (9)	12

List of Abbreviations

THG	Third Harmonic Generation
$\chi^{(3)}$	Third Order Nonlinear Optical Susceptibility
γ	Second Hyperpolarizability
HG	Harmonic Generation
SHG	Second Harmonic Generation
HHG	Higher Harmonic Generation
$(I_{3w})_g$	THG Intensity at the Glass-Air Interface
$(I_{3w})_{sol}$	THG Intensity at the Glass-Solution Interface
DFT	Density Functional Theory
HF	Hartree-Fock
TDHF	Time-dependant Hartree-Fock
LHCII	Light Harvesting Chlorophyll a/b Pigment-Protein Complex of Photosystem II
DBTD	4,7-dibromobenzo[c]-1,2,5-thiadiazole
AAA40	2-(2-phenylethenyl)-1H-pyrrole
AAA41	5-(2-Phenylethenyl)-1H-pyrrole-2-carboxaldehyde
THF	Tetrahydrofuran
LED	Light Emitting Diodes

2SIP	Outer-Outer-Sphere Solvent Ion Pair Structure
SIP	Outer-Sphere Solvent Ion Pair Structure
CIP	Inner-sphere solvent ion pair
MEP	Molecular Electrostatic Potential Plot

Chapter 1: INTRODUCTION

1.1 Research Overview

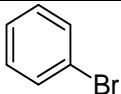
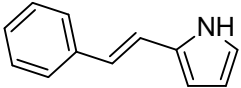
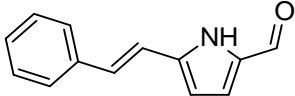
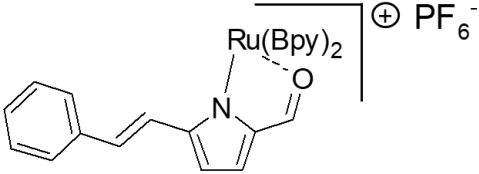
Third harmonic generation (THG) is a nonlinear optical effect where three photons from a laser simultaneously interact with a material to form one photon with three times the frequency of the laser photon.^{1,2} THG microscopy has been used to study non-biological and biological materials. Although less common than fluorescence microscopy, THG microscopy is advantageous for sample imaging as photobleaching from the promotion of electrons to an excited state does not occur.³ This is because unlike in fluorescence microscopy, incident photons are not absorbed.³ Due to this advantage over fluorescence microscopy, materials that generate strong THG signal – referred to as harmonophores – have attracted interest as dyes for THG microscopy.^{3–5} Potential harmonophores can be evaluated through comparing their third order nonlinear optical susceptibility ($\chi^{(3)}$) and second hyperpolarizability (γ) values. The $\chi^{(3)}$ values for a given molecule dissolved in solvent are concentration dependent and are related to the THG signal generated by the solution of interest.⁶ These values can be used to calculate the γ value of the molecule which is concentration independent.⁶ In this work, a systematic approach was used to study the effects that the level of substitution has on the observed γ values of a selection of organic and inorganic molecules. The effect that changing the base structure of a selection of pyrrole-containing ligands and ruthenium complexes has on their observed γ values was also studied.

1.2 Objectives of Thesis

This project aims to evaluate several series of aromatic compounds as potential harmonophores by using experimental methods to calculate their γ values. The compounds evaluated are the starting materials for two pyrrole compounds and the corresponding ruthenium complexes which will also be evaluated. Each compound has four in its series; the core starting

materials contain bromine functional group(s), two pyrrole containing species, and a ruthenium complex (Table 1).

Table 1. The bromobenzene based ruthenium complex series. This acts as a representative example for each of the starting materials evaluated in this work.

Starting Material	
Pyrrole 1	
Pyrrole 2	
Ruthenium-Pyrrole Complex	

The γ will be calculated using the $\chi^{(3)}$ values determined for the compounds. $\chi^{(3)}$ values for the compound dissolved in solvent are measured using the THG ratio method along with the refractive indices of the solutions at the fundamental laser wavelength, 1030 nm, and the third harmonic wavelength, 343 nm. The γ values for each compound will be compared to each other to evaluate the effects of increasing substitution on the systems. This study aims to look at how the functional groups present on the base compound influence the γ value observed. It also looks at how changing the core starting material influences the relative γ value observed for the metal complexes. This project has the overall goal of gaining a better understanding of how to optimize dyes for THG microscopy.

CHAPTER 2: BACKGROUND

2.1 Theory

2.1.1 Harmonic Generation Microscopy

Harmonic generation microscopy is a microscopy method that utilizes the nonlinear optical effect called harmonic generation (HG).⁶ In this effect, photons from an excitation beam simultaneously interact with a material to form one photon with higher frequency.⁶ There are different types of harmonic generation, which are differentiated based on the number of photons that combine when interacting with the material to generate the resulting photon.⁶ Common types of harmonic generation include second harmonic generation (SHG) and third harmonic generation (THG) (Figure 1).²⁶

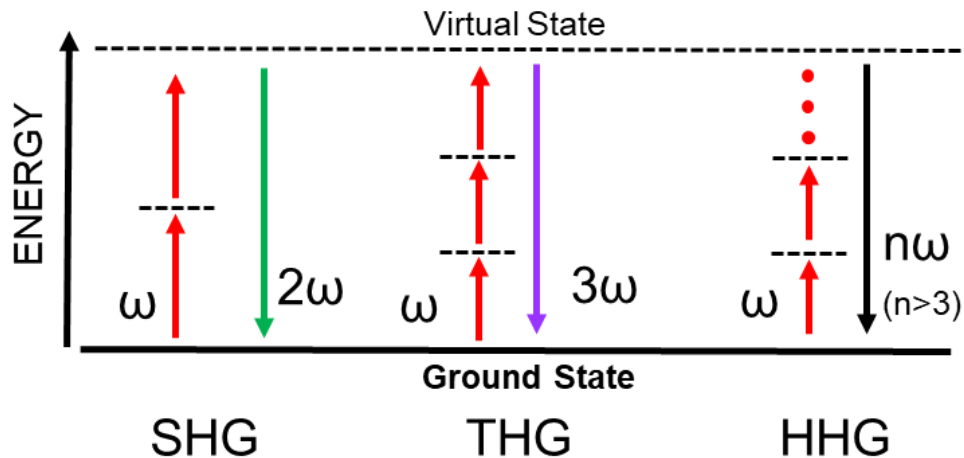


Figure 1. A pictorial representation of harmonic generation.⁶ SHG is depicted on the left, in which two photons combine to form a photon with twice the frequency (2ω).⁶ In the center, THG is depicted in which three photons combine to form a photon with three times the frequency (3ω).⁶ Higher harmonic generation (HHG) is represented on the right with the number of photons being represented by n , where n is greater than 3.

This nonlinear optical effect is dependent on the polarization and the electric field strength of the light.⁶ The polarization observed for a given material represents the induced dipole caused by the movement of electrons in response to the electric field of the light.⁶ In nonlinear optics, the polarization $\tilde{P}(t)$ depends on the power series of the electric field strength $\tilde{E}(t)$ as depicted in Equation 1.⁶

$$\tilde{P}(t) = \epsilon_0 [\chi^{(1)}\tilde{E}^1(t) + \chi^{(2)}\tilde{E}^2(t) + \chi^{(3)}\tilde{E}^3(t) + \dots + \chi^{(n)}\tilde{E}^n(t)] \quad (1)$$

In Equation 1, ϵ_0 is a constant referred to as the permittivity of free space. $\chi^{(n)}$ is the nth-order non-linear optical susceptibility.

When studying molecules, (μ) is used to represent the induced dipole moment.⁷ It is calculated in a similar fashion to polarization of a material, as it depends on the power series of the electric field strength as shown in Equation 2.⁷

$$\mu = \mu_0 + \alpha\tilde{E}^1 + \beta\tilde{E}^2 + \gamma\tilde{E}^3 + \dots \quad (2)$$

Where μ_0 is the static dipole moment, β is the first hyperpolarizability, and γ is the second hyperpolarizability.⁷ The average μ for the molecule can be used to calculate the polarization for molecules in a bulk solution (Equation 3).⁷

$$\tilde{P}(t) = \epsilon_0 N \langle \mu \rangle \quad (3)$$

$$\therefore \tilde{P}(t) = \epsilon_0 [N \langle \mu_0 \rangle + \tilde{E}^1(t)N \langle \alpha \rangle + \tilde{E}^2(t)N \langle \beta \rangle + \tilde{E}^3(t)N \langle \gamma \rangle + \dots]$$

Where the polarization represents the dipole moment per unit volume and N is the number density of the molecules.⁷

The order of $\chi^{(n)}$ depends on the number of photons that combine. $\chi^{(2)}$ is referred to as the second order nonlinear optical susceptibility and it represents the ability of a material to generate second order nonlinear optical processes, such as SHG.⁶ Likewise, the third order

nonlinear optical susceptibility, $\chi^{(3)}$, represents the ability of a material to generate third order nonlinear optical processes, such as THG.⁶ Large $\chi^{(3)}$ values indicate that a material is capable of generating strong THG signal.³ Molecules that generate strong THG signal are referred to as harmonophores.³ The $\chi^{(3)}$ values for solutions containing dissolved compounds are concentration dependent and can be used to determine the molecule's ability to generate a third order nonlinear optical process such as THG, refer to as γ .⁶ The γ value of a compound is concentration independent.⁶ It is reported in the literature and less often compared to $\chi^{(3)}$ values for compounds in solutions as it requires the concentration dependency of $\chi^{(3)}$ values, and refractive indices in order to be calculated.⁸ There are different ways that a material's $\chi^{(3)}$ values can be measured, including the Maker-fringe technique or the THG ratio technique.^{4,5,8,9} The THG ratio technique is useful in determining both the $\chi^{(3)}$ values and γ value for a given compound.

2.1.2 Second Harmonic Generation Microscopy

The first type of harmonic generation reported was SHG, shortly after the first working laser was established in the 1960s.⁶ In SHG two photons from the excitation beam simultaneously interact with a material to generate one photon with twice the frequency of the excitation beam (Figure 2).^{1,10}

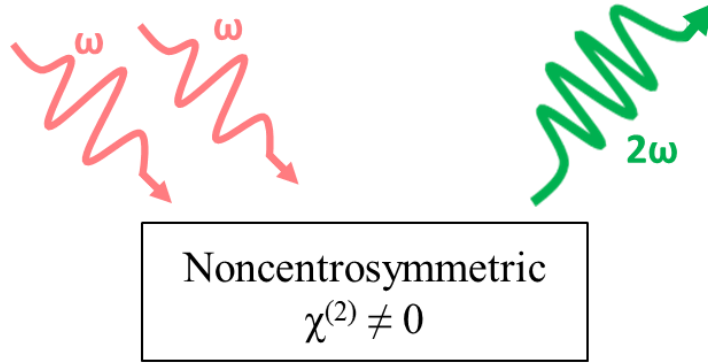


Figure 2. Combination of two photons with a given frequency when interacting with a noncentrosymmetric material to form a photon with twice the frequency of the excitation beam.

This effect involves the combination of two photons, which makes its nonlinear optical susceptibility second order.⁶ The induced polarization of a material $\tilde{P}(t)^{(2)}$ in relation to the second order nonlinear optical susceptibility can be determined using Equation 4.⁶

$$\tilde{P}(t)^{(2)} = \epsilon_0 \chi^{(2)} \tilde{E}^2(t) \quad (4)$$

The order of the nonlinear optical susceptibility plays a role in what materials can be studied using this technique. With second order and higher even order harmonic generation, one of the limitations of the effect is that it requires the material of interest to be noncentrosymmetric.⁶ This is due to the effect that squaring of the electric field strength has, as it causes $\tilde{P}(t)^{(2)}$ to be equivalent to $-\tilde{P}(t)^{(2)}$, as seen in the comparison of Equation 5.⁶

$$\begin{aligned} -\tilde{P}(t)^{(2)} &= \epsilon_0 \chi^{(2)} \left(-\tilde{E}(t)\right)^2 \\ &\equiv \tilde{P}(t)^{(2)} = \epsilon_0 \chi^{(2)} \tilde{E}^2(t) \\ \therefore \tilde{P}(t)^{(2)} &= -\tilde{P}(t)^{(2)} \end{aligned} \quad (5)$$

Centrosymmetric materials cannot be studied with SHG since $\tilde{P}(t)^{(2)}$ is equivalent to $-\tilde{P}(t)^{(2)}$, which results in the polarization canceling out and the second order non-linear optical susceptibility equalling zero.⁶

Although SHG is limited to noncentrosymmetric materials, it does provide advantages over other commonly used techniques such as fluorescence and atomic force microscopy.¹⁰ These advantages include that it is a fast, label free technique, which is non-invasive and does not damage the samples when scanned.¹⁰ It has been used to study biological materials including starch, collagen fibres, and cancerous tissues.¹⁰⁻¹³ Starch has been studied using SHG microscopy, where the A- and B-type allomorphs can be distinguished based on their SHG generated.¹³ The effects on the SHG intensity for heat treated starch granules have also been studied.¹⁴ In this, the SHG intensity decreases over time as the sample is heated.¹³ Collagen fibre has also been studied using SHG microscopy, in which orientation has been observed to affect the SHG signal generated.¹¹ Following this, cancerous tissue has also been studied; one study looked at ovarian cancer.¹² In this study, differences in the collagen fibre of normal tissue, benign tumors, stage III and stage IV cancerous tissue were compared.¹² In this, differences in the SHG signal generated by the non-cancerous and cancerous tissue collagen were observed.¹² No significant difference was observed between the stage III and IV cancerous tissue collagen.¹²

There are other types of HG microscopy, such as THG microscopy. This type provides an advantage over SHG as it can be used to study more materials as it does not require non-centrosymmetry.²

2.1.3 Third Harmonic Generation Microscopy

THG is a nonlinear optical process where three photons from a laser interact simultaneously with a material to generate one photon with three times the frequency of the excitation beam.^{1,2}

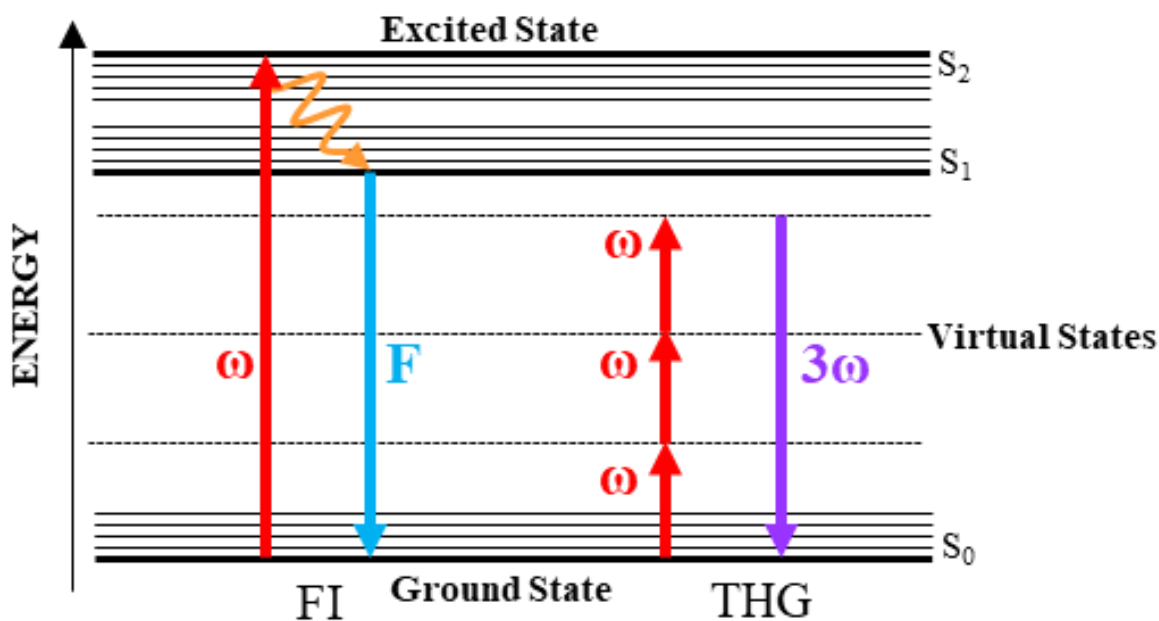


Figure 3. A comparison of fluorescence (FI) and THG. FI involves the absorption of a photon with a given frequency (ω), a Stokes shift of the excited electron (orange arrow), and emission of a lower energy photon (F). THG involves the combination of three photons with a given frequency (ω) to generate a photon with three times the frequency (3ω). This process does not occur at the excited state but rather at a virtual state.

As depicted in Figure 3, single photon fluorescence involves the absorption of a single photon by a compound and promotion of an electron to an excited state. Some energy is lost as heat when the electron transitions to a lower excited state, which is referred to as a Stokes shift.¹⁵ Following this, the electron returns to the ground state and a photon with lower energy than the

initial photon is emitted. Photodamage can occur during the Stokes shift and while the compound is in an excited state.^{3,15} In fluorescence microscopy one way that damage to the sample - referred to as photobleaching - can occur is through the formation of oxygen radicals.³ The risk of damage to a sample during imaging poses a limitation for fluorescence microscopy application to study samples for *in-vivo* studies. THG microscopy provides an advantage over this technique as it does not cause photobleaching of the sample.³ This is because electrons are not promoted to the excited state thus no Stokes shift occurs. This makes THG microscopy a desirable technique for cell imaging, specifically for *in-vivo* studies. This technique has been used to study salt solutions, biological molecules, and non-biological molecules.^{3,8,16,17} One limitation of this technique is that the compound of interest must have an interface with a material that has a different refractive index or $\chi^{(3)}$ in order for its THG signal to be detected.^{5,8} This is due to destructive interference of the THG signal caused by an effect called the Gouy phase shift as depicted in Figure 4.^{8,18} The Gouy phase shift causes light on the left-hand side of the laser focal volume to be out of phase by π radians with the light on the right-hand side of the laser focal volume. As a result, THG signal that is generated on the left-hand side of the laser focal volume cancels the THG signal produced on the right-hand side of the laser focal volume due to total destructive interference.^{8,18}

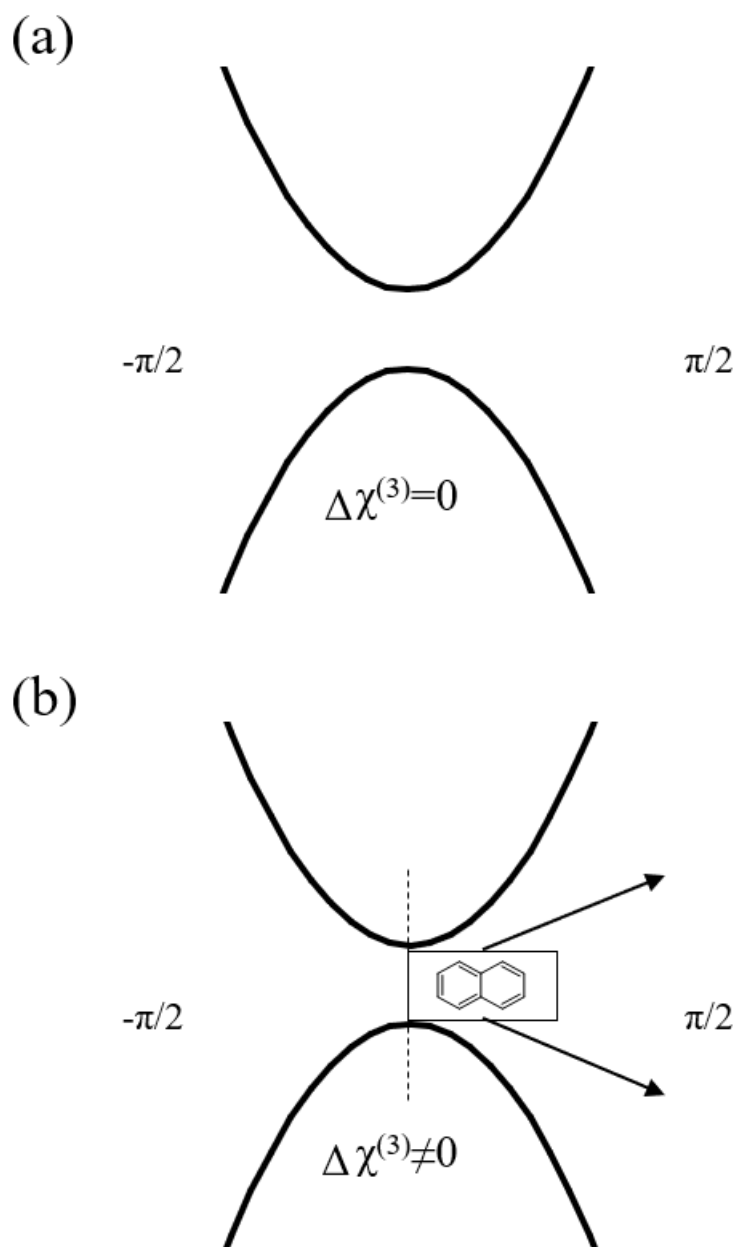


Figure 4. Depiction of the Gouy phase shift (a) where the THG signal produced on either side is cancelled out due to a phase shift in π radians. The breaking of the focal volume symmetry (b) is represented by the arrows coming from the rectangle around the compound of interest. The rectangle represents an interface between a sample and a surrounding material.

One of the ways that this issue can be addressed is by breaking the focal volume symmetry using an interface such as interfaces introduced by a glass capillary tube.^{5,8} In this method, the THG intensities of the glass-air $(I_{3\omega})_g$ and glass-solution $(I_{3\omega})_{soln}$ interfaces are measured and the equation by Schcheslavskiy *et al.* is used to calculate the $\chi^{(3)}$ ratio, as shown in Equation 6.^{8,19}

$$\frac{(I_{3\omega})_{soln}}{(I_{3\omega})_g} = \frac{|(n_{3\omega})_{soln} \chi_g^{(3)} J_g + (n_{3\omega})_g \chi_{soln}^{(3)} J_{soln}|^2}{((n_w^3)_g (n_{3\omega})_g (n_{3\omega})_{soln}) |\chi_g^{(3)} J_g|^2} \quad (6)$$

In this, n represents the refractive index at the fundamental frequency (ω) and THG frequency (3ω) for the solution (soln) or glass (g). The phase matching integrals are represented by J . The third order nonlinear susceptibility of the solution and glass are represented by $\chi^{(3)}$.

THG microscopy in combination with the refractive index can also be used to calculate the $\chi^{(3)}$ values of materials. These values then can be used to derive the second hyperpolarizability (γ) value for the solvent and the molecule of interest. The $\chi^{(3)}$ for solutions is calculated using Equation 7.^{8,20}

$$\chi^{(3)} = \left(\frac{n_w^2 + 2}{3}\right)^3 \left(\frac{n_{3\omega}^2 + 2}{3}\right) (N_s \gamma_s + N_{sol} \gamma_{sol}) \quad (7)$$

In this equation, number density is represented by N for the solvent (sol) and solute (s). Following this, the $\chi^{(3)}$ values are plotted against the concentration of the solutions in order to calculate γ .⁸ The γ_{sol} is calculated using the intercept of the line, while γ_s is calculated using the slope of the line.⁸

2.1.4 Refractive Index

Refractive indices are used to calculate the $\chi^{(3)}$ and γ values for THG microscopy. The refractive index at a given concentration is measured using Snell's law (Equation 8), where the refractive index of the initial medium n_1 multiplied by the sine of the angle of incidence θ_1 is equal to the refractive index of the second medium n_2 multiplied by the sine of the angle of transmission θ_2 .²¹

$$n_1 \sin \theta_1 = n_2 \sin \theta_2 \quad (8)$$

Another form of Snell's law, shown in Equation 9, depicts the relationship between the critical angle (θ_c) and the refractive indices of the two media.²¹

$$\theta_c = \arcsin \frac{n_1}{n_2} \quad (9)$$

There are multiple different methods that are used to measure refractive index, some of which include: deviation methods, Brewster angle method, and the index match method. One of the more common methods used is the critical angle method.²¹ For liquid samples, an Abbe refractometer is used to record the measurements by first placing the sample between two prisms with a known refractive index.²¹ Light at a known wavelength is then passed through the prisms and the critical angle for the solution can then be determined either through transmission or reflection.²¹ Transmission is the most common method, where the critical angle is found by taking the maximum angle of transmission observed for the solution when light is passed through the prisms.²¹ One alternative to the Abbe refractometer which has been used to measure the refractive indices of solutions for the THG ratio technique is a tuneable refractometer. In this, the refractive index at both the fundamental laser wavelength and the third harmonic wavelength are calculated for the solutions.

2.2 Literature Review

2.2.1 Introduction

THG microscopy has been explored as a potential technique to study cancerous tissue and tumors.^{22,23} This technique has also been used to evaluate nonlinear optical properties of biological and nonbiological compounds.^{3,24} Both the $\chi^{(3)}$ and γ values of materials have been studied, although $\chi^{(3)}$ values are reported more often because the refractive indices of the material are required when calculating for the γ value.⁸ In this field, nonbiological compounds have been studied using this technique for their potential use in nonlinear optics and electronics.^{9,25} One of the focuses of these studies is what the influence that additional functional groups and extension of conjugation has on the THG signal generated by the compounds.^{26,27} These studies aim to optimize the compounds by increasing their γ value. Additionally, computational calculations for $\chi^{(3)}$ and γ values are commonly found alongside the experimentally determined values in these studies. Computational chemistry plays an important role in THG microscopy as there has been extensive work on calculating the γ values for both biological and non-biological compounds.^{9,28–30} This is because it allows for the nonlinear optical properties of the compounds to be investigated without the need for the equipment required to study them experimentally.

Biological compounds have been evaluated using this technique to see if they could act as potential dyes for tissue staining in THG microscopy.^{3–5,8,31} Within studies of both biological and non-biological compounds, one shared goal has been to learn about what improves the observed THG signal. This is done by optimizing the compounds to increase the THG signal observed, which in turns improves compounds for applications such as staining, electronics, and non-linear optics.^{3,30,32}

2.2.2 Non-biological Harmonophores in THG Microscopy

THG microscopy has been used to evaluate a range of different non-biological compounds including simple aromatic molecules, highly conjugated systems, and metal complexes.^{17,27,33,34} This is done with the goal of better optimizing compounds to give off stronger THG signal for uses in areas such as dyes, nonlinear optics, and electronics.^{9,16,17,26} These studies have either experimentally or computationally determined the $\chi^{(3)}$ and γ values for these compounds. In these studies, the effect of push-pull systems and the level of conjugation present in the compounds of interest have been evaluated.^{25,35,36}

Reinhardt *et al.* evaluated both the $\chi^{(3)}$ and γ values for a series of benzobisthiazole, benzobisoxazole, and benzobisimidazole compounds.²⁶ The calculated γ values from this study were found to have a correlation with the level of conjugation present in the compounds.²⁶ This agrees with Balu *et al.* and Motomura *et al.* who also reported that the amount of conjugation present for a compound influences the γ value observed, with larger γ values being associated with increases in conjugation.^{27,37} Additionally, Reinhardt *et al.* found that the addition of electron withdrawing groups increased the γ value observed.²⁶ This was attributed to how the electron withdrawing group decreases the optical bandgap which increases the rate at which photons can be absorbed.²⁶ One limitation of this work which was noted is that a high level of error was reported for the calculated γ values.²⁶

Push-pull systems are compounds that contain both an electron withdrawing group and electron donating group within the same π system. Sakki *et al.* focused on determining the γ values for a series of push-pull dicyanovinylbenzene compounds.⁹ 2-benzylidenemalononitrile, 2-(4-chlorobenzylidene)malononitrile, 2-(4-hydroxybenzylidene)malononitrile, and 2-(4-(dimethylamino)benzylidene) (Figure 5) were analyzed.⁹

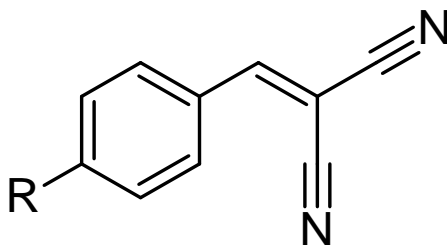


Figure 5. The molecular structure for the dicyanovinylbenzene compounds, where R = -H, -Cl, -OH, -N(CH₃)₂.⁹

2-(4-hydroxybenzylidene)malononitrile was found to have the largest γ value, although all the values were within an order of magnitude to each other.⁹ This was attributed to the presence of its hydroxyl group (-OH) which acts as an electron donor.⁹ This indicates that electron donor groups influence the THG intensity observed for compounds.⁹

Mydlova *et al.* also studied push-pull systems, focusing on a series of 4 compounds containing sulfur heterocycle 2,2'-bis(1,3-dithiolylidene).²⁵ These compounds were broken up into two groups, one group had nitro group substituents and the other had methyl substituents (Figure 6).²⁵

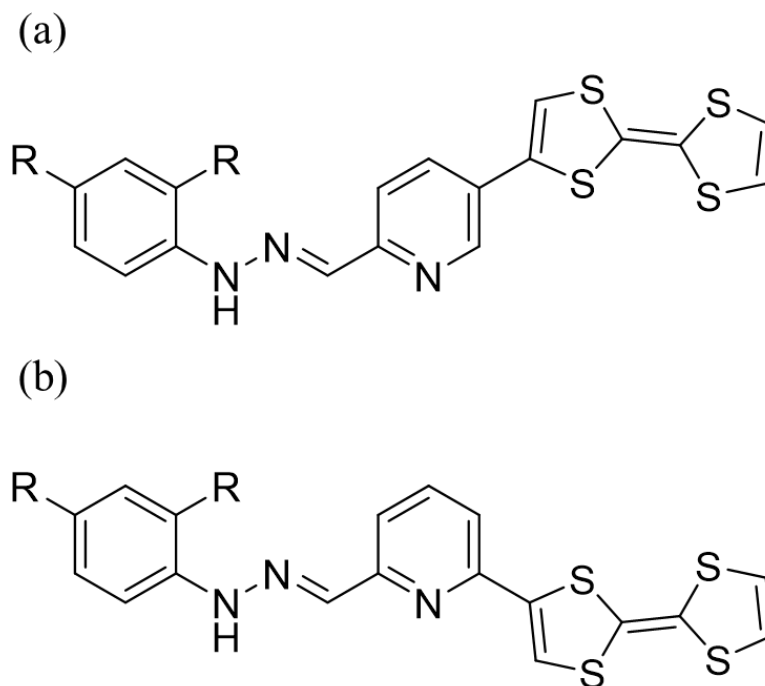


Figure 6. The molecular structure for the tetrathiafulvalene-appended azine ligands, where R = $-\text{NO}_2$, CH_3 .²⁵

In each group, the only difference between the compounds was that one was para-substituted and the other was meta-substituted.²⁵ Only the $\chi^{(3)}$ values were calculated and compared for the compounds. In this study, the compounds' substituents had a minor influence on the $\chi^{(3)}$ value observed, although the compounds with nitro groups had a higher $\chi^{(3)}$ value.²⁵ The type of substitution played a greater role in the $\chi^{(3)}$ value observed, where higher $\chi^{(3)}$ values were observed for the para-substituted compounds.²⁵ This indicates that the substitution pattern influences THG intensity.²⁵ This disagrees with the results reported in Papagiannouli *et al.* where the $\chi^{(3)}$ values of six push-pull type pyrazoline derivatives were determined.³⁸ In this study, no correlation between the position of the nitrile and nitro groups and the $\chi^{(3)}$ value observed for the compounds was found.³⁸ The compounds with the nitro groups were found to have a higher $\chi^{(3)}$ value than when the nitrile groups were present.³⁸ This may be because the nitro groups act as

stronger electron acceptors compared to the nitrile groups.³⁸ This agrees with the findings from Sahki *et al.* where the presence of nitro groups on 2-aryl-1H-phenanthro[9,10-d]imidazole compounds also increased the $\chi^{(3)}$ value observed.³⁰

Non-biological compounds that are common dyes have also been investigated using THG microscopy. Ramos-Ortiz *et al.* determined $\chi^{(3)}$ values for the dyes crystal violet and ethyl violet.¹⁶ These compounds differ from push-pull systems as they are octapolar instead of dipolar.¹⁶ In this, they have three electron donating groups which are bonded to a central electron deficient carbon atom.¹⁶ In this study, the $\chi^{(3)}$ values for crystal violet and ethyl violet were determined to be similar. This is despite ethyl violet having a slightly stronger donating group.¹⁶

2.2.3 Computational Studies on Potential Harmonophores

Computational studies have been performed on both biological and non-biological compounds to calculate their $\chi^{(3)}$ and γ values. The most common methods used to calculate $\chi^{(3)}$ and γ values include Density Functional Theory (DFT) and Hartree-Fock (HF).^{9,30,39} Initial studies that aim to calculate these values computationally focused on simple aromatic molecules. Balu *et al.* focused on several simple aromatic molecules, which included benzene and naphthalene.²⁷ The γ values of these molecules were calculated and compared using time-dependent Hartree-Fock (TDHF) method.²⁷ From their results they concluded that the number of rings present in the structure highly influenced the γ values observed.²⁷ Additionally, they observed that the direction in which additional rings were added had a minor effect on the γ value.²⁷

Further studies have focused on biological compounds and more complex non-biological compounds. For biological compounds the γ values for amino acids has been determined computationally. Tokarz *et al.* calculated the γ values for amino acids using the TDHF method.²⁸ Serine and threonine were found to have the lowest γ values.²⁸ The amino acid types with the

largest γ values include the aromatic amino acids and those with second carboxylic acids. For the aromatic amino acids, this was attributed to high levels of conjugation.²⁸ This agrees with Reinhardt *et al.* and Balu *et al.* where conjugation was also observed to influence γ .^{26,27} For the second carboxylic acids, their large γ values were attributed to electron delocalization of the additional carboxylates.²⁸

Sofiani *et al.* used both experimental and computational methods to study the non-linear optical properties of 7-amino-2-p-tolyl-2H-thiazolo[3,2-a]pyrimidine-3,5-dione and (E)-methyl 2-amino-4,5-dihydro-4-p-tolylpyrido[3,2-b][1,4]oxazepine-3-carboxylate (Figure 7).⁴⁰

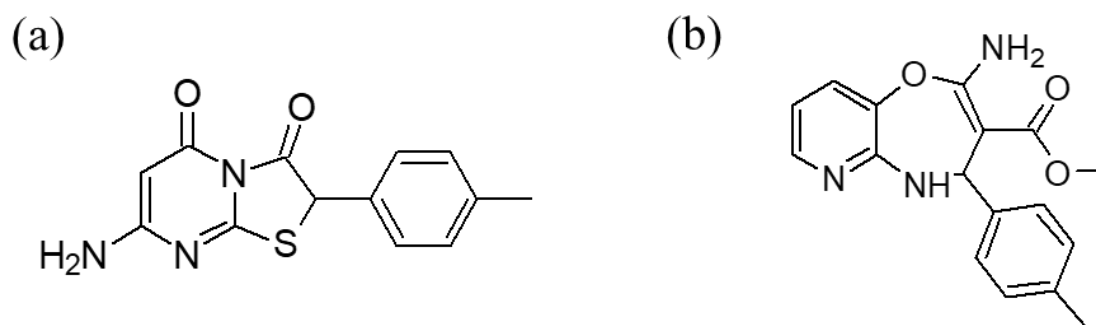


Figure 7. The molecular structure for 7-amino-2-p-tolyl-2H-thiazolo[3,2-a]pyrimidine-3,5-dione (a) and (E)-methyl 2-amino-4,5-dihydro-4-p-tolylpyrido[3,2-b][1,4]oxazepine-3-carboxylate (b).

40

The γ values for the compounds was calculated using the HF method.⁴⁰ (E)-methyl 2-amino-4,5-dihydro-4-p-tolylpyrido[3,2-b][1,4]oxazepine-3-carboxylate was found to have a significantly larger γ value which was attributed to its stronger dipole moment.⁴⁰ One limitation to the computational calculations that this paper noted was how the interactions between molecules was not accounted for which could give rise to error for the calculated values.⁴⁰ Another study focused on the effect that bromine substitution had on the THG signal generated by 2,3-

dimethoxybenzaldehyde derivatives.³³ Aguiar *et al.* determined the γ values for 2,3-dimethoxybenzaldehyde, 5-bromo-2,3-dimethoxybenzaldehyde, and 6-bromo-2,3-dimethoxybenzaldehyde computationally using coupled perturbed HF method.³³ 5-bromo-2,3-dimethoxybenzaldehyde was reported to have a slightly higher γ value than 6-bromo-2,3-dimethoxybenzaldehyde indicating that the position of the bromine functional group has a minor influence on γ values.³³ The addition of the bromine functional group compared to the unsubstituted 2,3-dimethoxybenzaldehyde gave rise to an increase in the γ value observed regardless of its position on the ring.³³

2.2.4 Biological Compound Based Harmonophores in THG Microscopy

Biological molecules have been found to be promising dyes for THG microscopy, specifically for *in-vivo* studies, as they are often biologically compatible.^{5,8} Some examples of biological molecules that have been investigated previously include carotenoids and chlorophylls.^{3,8} Carotenoids were investigated as a potential *in-vivo* dye for THG microscopy, and were studied in *Drosophila melanogaster* larvae.³ The carotenoid compounds that were evaluated included: Violaxanthin, Neoxanthin, Lutein, Zeaxanthin, Canthaxanthin, Astaxanthin, and β -carotene. From this study, they found that β -carotene was an effective dye as it significantly increased the THG intensity observed in the larvae.³ The structure of β -carotene is shown in figure 8. The γ value of β -carotene was determined to be $7100 \pm 400 \times 10^{-44} \text{ m}^2 \text{V}^{-2}$.⁸

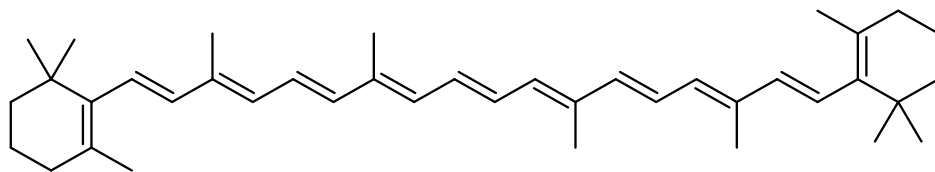


Figure 8. The molecular structure of β -carotene.⁸

The γ value for β -carotene has been used as a reference to evaluate compound potential as a dye for THG microscopy.^{3,5} When comparing the γ values for the carotenoids it was reported that epoxide functional groups and increased conjugation caused a rise in the γ value.³ This was in agreement with what a previous study had observed where chain length of the carotenoids was seen to have an influence on the γ value.³⁶

Chlorophylls have also been investigated; negative γ values were observed for chlorophyll a and chlorophyll b.⁸ The negative γ values were attributed to a phase difference in the THG being emitted, where the chlorophylls were opposite in phase compared to the solvent they were dissolved in.⁸ This agrees with the results reported by Sun *et al.*³¹ Chlorophyll a was reported to have a slightly larger γ value than Chlorophyll b.⁸

Nonlinear optical properties of light-harvesting complexes have been investigated using THG microscopy. In one study, the γ value of light harvesting chlorophyll a/b pigment-protein complex of photosystem II (LHCII) was determined experimentally.⁴ LCHII contains chlorophyll a and b along with carotenoids, which both contribute to the complexes γ value.⁴ Its γ value was reported as $-1600000 \pm 400000 \times 10^{-44} \text{ m}^2\text{V}^{-2}$.⁴ As part of this study, the effect of having a solution of compounds with negative and positive γ value was assessed.⁴ This was evaluated by measuring the γ value for a 20:1 ratio mixture of chlorophyll a, which has a negative γ value, and β -carotene, which has a positive γ value, in acetone.⁴ In this, it is reported that THG generated was effectively cancelled out due to the γ value of the carotenoids being opposite in sign to chlorophyll a.⁴ This showed that the sign of the γ value of a potential dye should be considered when placing it in the presence of other compounds that generate THG signal. Another study looked at the light-harvesting complexes called phycobiliproteins.⁵ This study aimed to determine the THG generated by the complexes to evaluate their potential use as dyes for THG microscopy.⁵ In this, CL-

allophycocyanin, C-phycocyanin, and R-phycoerythrin γ values were determined experimentally.⁵ CL-allophycocyanin, C-phycocyanin, and R-phycoerythrin all had negative γ values indicating that they were in opposite phase of the solvent.⁵ R-phycoerythrin was reported to have the largest γ values which was larger than β -carotene indicating that it can be potentially used as a dye for THG.⁵

Chapter 3: EXPERIMENTAL

3.1 Materials

Analytes used for this study include: Bromobenzene, 1,4-dibromobenzene, 1,4-dibromothiodiazole, naphthalene, 2-bromonaphthalene, 2,6-dibromonaphthalene and 4,7-dibromobenzo[c]-1,2,5-thiadiazole (DBTD). They were purchased by Dr. Allison Thompson's group at Dalhousie University and given to Dr. Tokarz's research group for analysis. Additionally, Dr. Alison Thompson's group synthesized 2-(2-phenylethenyl)-1H-pyrrole (AAA40) and 5-(2-phenylethenyl)-1H-pyrrole-2-carboxaldehyde (AAA41), which were also given to Dr. Tokarz's research group for analysis. Tetrahydrofuran (THF) with 0.025% butylated hydroxytoluene (BHT) stabilizer was purchased from Fisher Scientific. Magnesium sulfate heptahydrate (M-0900 ACP Chemical) was also used as an analyte.

3.2 Experimental Determination of γ Values

3.2.1 Solution Preparation

Solutions were prepared in ambient conditions at $21 \pm 1^\circ\text{C}$ and $30 \pm 10\%$ humidity. Stock solutions were prepared in glass vials. A known quantity of the analyte was dissolved in 1.000 ± 0.001 mL of THF. Increasing amounts of stock solution were then pipetted into glass vials which was followed by the addition of 1.000 ± 0.001 mL of tetrahydrofuran (THF) to each. The dilute solutions were prepared with within the millimolar concentration range. Each series contained 4 increasing concentration solutions, except for naphthalene which only had a series of 3 solutions. The vials were capped and sealed with parafilm between measurements to reduce loss of solvent due to evaporation. If the solution measurements were completed on two separate days, the vials were capped, sealed with parafilm, and stored at -18°C to reduce evaporation. Salt solutions were prepared using a slightly different method where the salt solutions were diluted

with 1.000 ± 0.001 mL of deionized water. Salts that were used include magnesium sulfate and sodium chloride. The salt solutions were prepared at a molar concentration which was higher than the dilute solution concentration for the starting materials and pyrrole compounds. The salt solutions were stored at 4°C between measurement days.

3.2.2 Refractive Index Measurements

Refractive indices for each analyte were taken using a home-built UV to near IR refractometer using the previously described set-up by Purvis *et al.*⁵ The refractometer (Figure 9) is equipped with two light emitting diodes (LED); one at 340 nm (M340L4, Thorlabs Inc.) and the other at 1050 nm (M1050L2, Thorlabs Inc.) with a bandwidth of 60 nm. An optical filter (FLH1030-10, Thorlabs Inc.) is attached to the 1050 nm LED to control the bandwidth to obtain light at 1030 nm for measurements. When collecting the measurements, the solutions were added into a butyl rubber spacer (Seal & Design Canada) which was pressed between two yttrium aluminum garnet prisms (Red Optronics). A standard CMOS camera (HD Webcam C270, Logitech) was used to detect the transmitted light from the solutions.

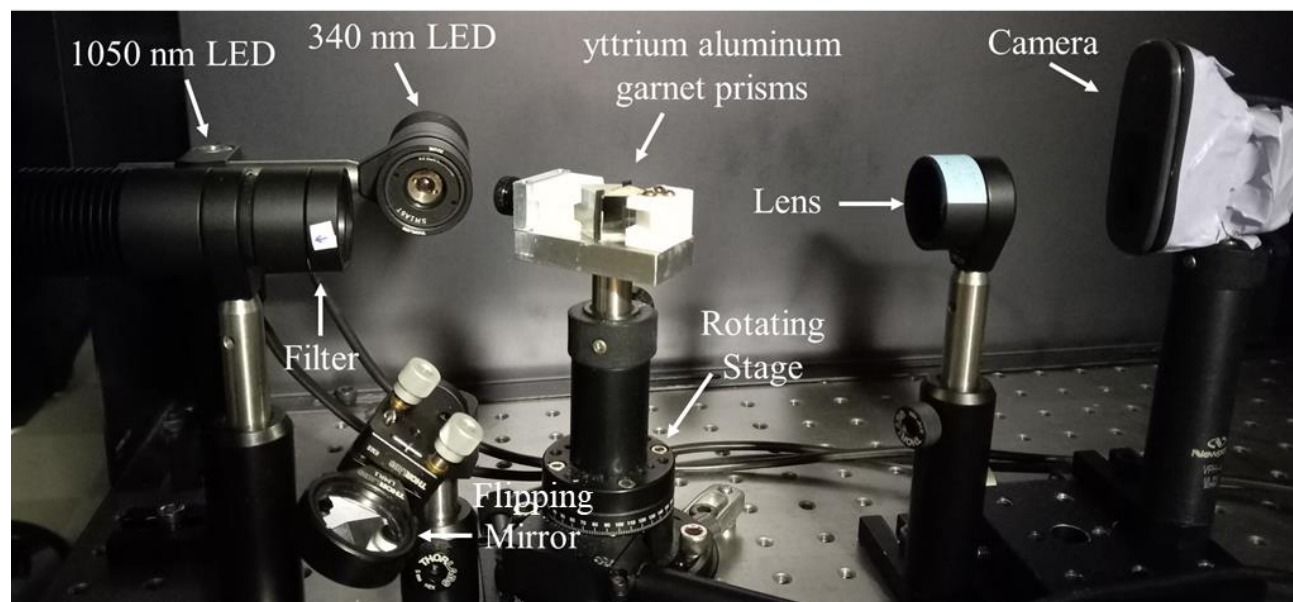


Figure 9. Labelled image of the home-built UV to near IR tunable refractometer.

The measurements were collected at $21 \pm 1^\circ\text{C}$ in low light conditions. During the measurements, the diluted solution prepared was pipetted into the spacer region of the prisms using a micropipette. Following this, the solution in the prisms were rotated using the rotating stage until the total internal reflection is detected. The critical angles for both the solvent and analyte solution were then collected. The angles were then used to calculate for the refractive index at that given concentration. This is done by calculating the difference between the critical angle of the analyte solution and the solvent. After measurements were collected for a given analyte, acetone was used to clean the prisms before measurements were collected for another compound.

3.2.3 THG Intensity Ratio Measurements

THG intensity ratio measurements were collected for each solution using a homebuilt nonlinear optics microscope equipped with a 1030 nm femtosecond duration pulse laser (Figure 10). The laser set-up is similar to what has been previously described.^{4,5} A 0.3 numerical aperture (NA) air immersion microscope objective lens was used to focus the laser beam onto the sample.

The samples' THG signal was collected by a custom polarization independent 0.85 NA collection objective lens (Omex Technologies USA). After passing through a filter (65-129, Edmund Optics Inc.) the signal was detected by photon counting photomultiplier tubes.

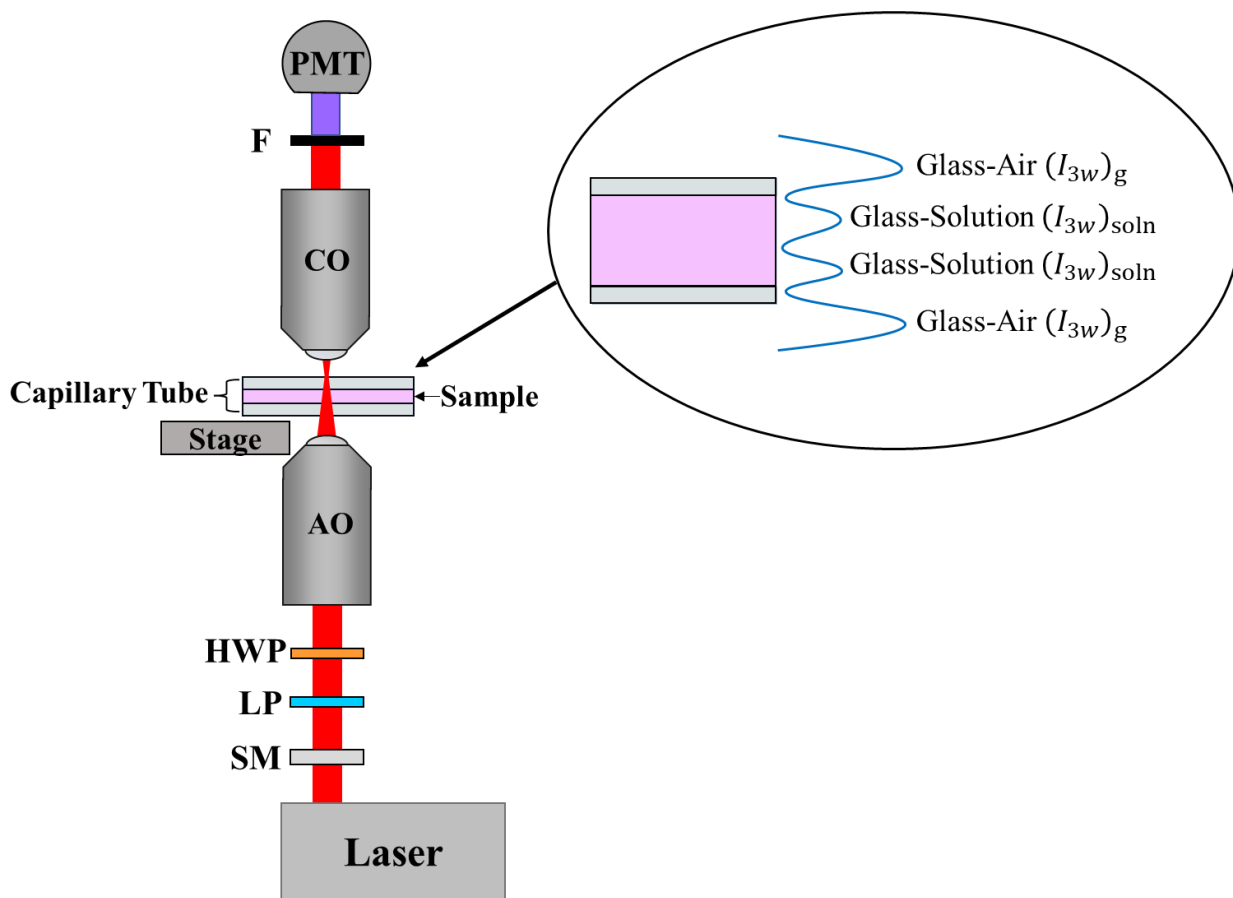


Figure 10. Schematic of homebuilt nonlinear optical THG microscope with pictorial representation of the different interfaces. Abbreviations: SM (Scanning Mirrors), LP (Linear Polarizer), HWP (Half-Wave Plate), AO (0.3 NA Air Immersion Objective), CO (0.85 NA Collection Objective), F (Filter), PMT (Photomultiplier Tube Detector)

Solutions were left to equilibrate to ambient temperatures before being used to prepare samples for the measurements. The samples were prepared by taking up a small amount of solution

into a borosilicate glass capillary tube (VitroCom) which was then sealed with clear nail polish. Once the nail polish dried the sample was then placed into the microscope vertically above the objective and 10 scans were collected at $21 \pm 1^\circ\text{C}$ for each sample. The scans were collected at a laser power of 10mW. The collected THG intensity ratios were then used along with the refractive indices of the solutions to calculate χ^3 by applying Equation 6 described by Shcheslavskiy *et al.*¹⁹ The χ^3 values for each solution were calculated using a custom The calculated χ^3 values were then plotted against the concentration of the samples to calculate for γ in Excel. The γ value for the solvent was calculated using the intercept of the line and the γ value for the analyte was calculate using the slope of the line.

Chapter 4: RESULTS AND DISCUSSION

4.1 Salt Solutions

Initial measurements were performed on sodium chloride solutions, for which deionized water was used as the solvent. These were performed in replication of previous work using sodium chloride which determined γ to be $2.1 \pm 0.5 \times 10^{-44} \text{ m}^2 \text{V}^{-2}$.⁸ In Figure 11, the refractive indices of the sodium chloride solutions are shown at 1030 nm and 343 nm. The experimentally determined values appear to closely match those obtained in a previous study.⁸ Additionally, the THG ratio data collected for the sodium chloride solutions is shown in Figure 11, along with the calculated $\chi^{(3)}$ values. The experimentally determined γ of the sodium chloride solutions is $1.7 \pm 0.2 \times 10^{-44} \text{ m}^2 \text{V}^{-2}$, which falls within the range of the previously determined value.

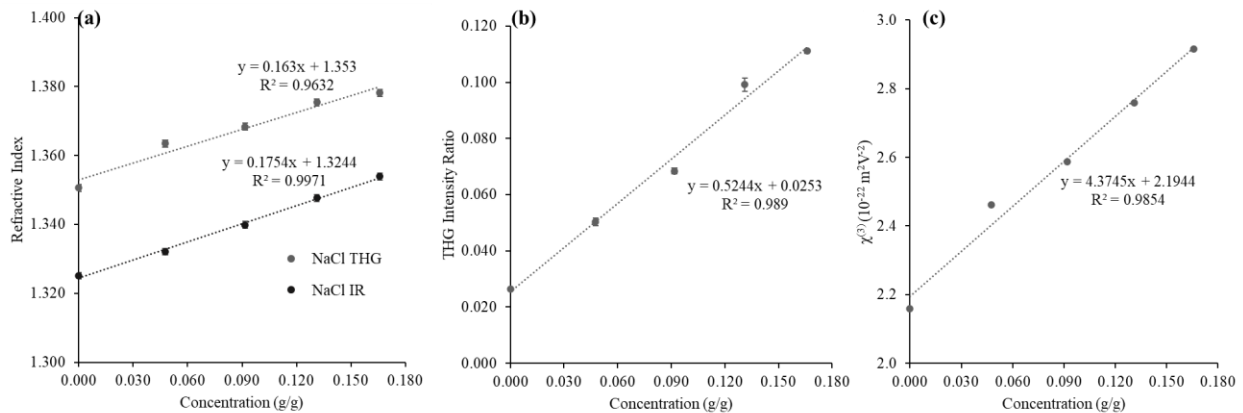


Figure 11. The refractive indices and THG intensity ratios used in the determination of the second hyperpolarizability value for NaCl. The refractive indices taken at 343 nm (THG) and 1030 nm (IR) (a), the THG intensity ratios (b), and the third order nonlinear susceptibility values (c) plotted over the concentration of the NaCl solutions. Errors bars are given for each graph.

Following these measurements, aqueous MgSO_4 solutions were evaluated. The refractive indices at 343 and 1030 nm as well as THG intensity ratios for the aqueous MgSO_4 solutions were

measured and used to calculate the $\chi^{(3)}$ values (Figure 12). The γ value for MgSO_4 could not be calculated due to the shift in the slope observed in the THG intensity ratio values.

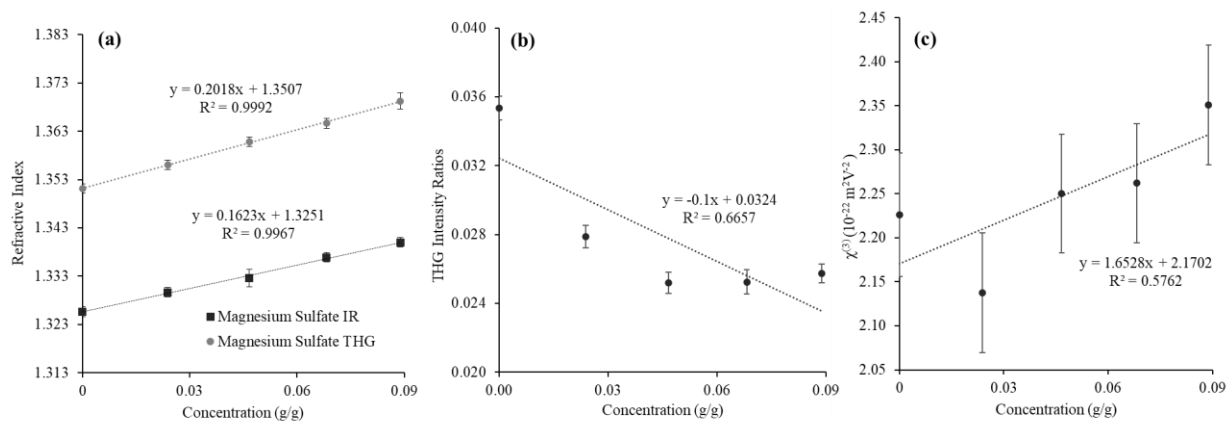
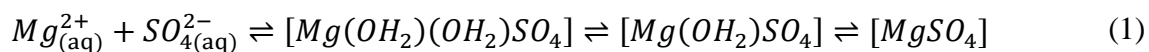


Figure 12. The refractive indices taken at 343 nm (THG) and 1030 nm (IR) (a), the THG intensity ratios (b), and the third order nonlinear susceptibility values (c) plotted over the concentration of the MgSO_4 solutions.

MgSO_4 behaved differently than what was observed for the NaCl solutions. In Figure 12, the THG intensity ratio values appear to behave non-linearly; a change in slope is observed at ~ 0.05 g/g (0.6 M). The change in slope may be from a concentration-dependent transition in the solvent shell of the MgSO_4 . This is based on the eigen mechanism which is a three-step equilibrium process based on the interaction between metal ion pairs and the solvent.^{41,42} This mechanism is shown in Scheme 1 for aqueous magnesium sulfate. The free ions first form a two-layer solvent shell around the metal ion referred to as the outer-outer-sphere solvent ion pair (2SIP) structure.^{41,42} As the ratio of ions to solvent increases there is only one solvent shell present around the metal ion which is called the outer sphere solvent-ion pair (SIP) structure.^{41,42} As the ratio between the ions and solvent increases even more the last structure that occurs is the inner-sphere solvent ion pair (CIP) where one of the coordinating solvent molecules is replaced by the anion.^{41,42}



Free ions

2SIP

SIP

CIP

Previous literature for $MgSO_4$ has reported that a shift in the equilibrium towards the CIP structure occurs once the concentration of $MgSO_4$ has reached around 0.4 M.⁴² An illustration of the change in equilibrium between the SIP to CIP structure for aqueous $MgSO_4$ solutions is shown in Figure 13.

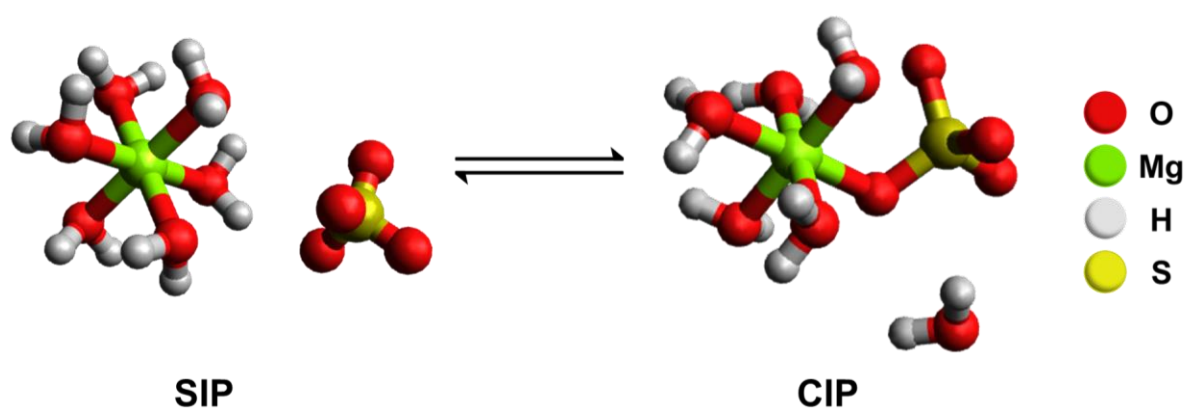


Figure 13. The solvent shell for magnesium and sulfate ions in water in the SIP and CIP structure.⁴¹

The transition occurs at a similar concentration to the concentration at which the change in slope is observed for the THG intensity ratios. This could mean that the change in the solvent shell of the $MgSO_4$ is being observed. Further studies on different salt solutions that undergo a similar solvent shell change should be completed to investigate this effect.

4.2 Starting Material Core Compounds

4.2.1 Benzene Ring Cores

Initial measurements were performed on a brominated benzene series, compounds included in this series were bromobenzene and 1,4-dibromobenzene. These compounds act as the starting material cores for the larger dye molecules, where the bromine functional group(s) was replaced with pyrrole-containing group. The bromobenzene solutions were prepared at a higher concentration than the 1,4-dibromobenzene solutions as at lower concentrations it was below the limit of detection. The refractive indices at 343 (THG) and 1030 (IR) nm (Figure 14a,d) and THG intensity ratios (Figure 14b,e) were taken for each solution. These values were used to calculate the $\chi^{(3)}$ values which were then plotted against their concentrations to calculate γ (Figure 14c,f).

The γ value of bromobenzene was calculated to be $-60 \pm 2 \times 10^{-44} \text{ m}^2\text{V}^{-2}$ and the solvent γ value was calculated to be $1.7 \pm 0.5 \times 10^{-44} \text{ m}^2\text{V}^{-2}$ (Table 2). The presence of a negative γ value indicates that bromobenzene is in opposite phase compared to the solvent, THF. Additionally, the bromobenzene γ value is $\sim 36\times$ greater in magnitude than the γ value of the solvent. The THG intensity ratios exhibited a small change from that of the solvent with a high level of deviation from linearity (Figure 14b). This indicates that the major contributor to the γ value is the refractive indices of the bromobenzene.

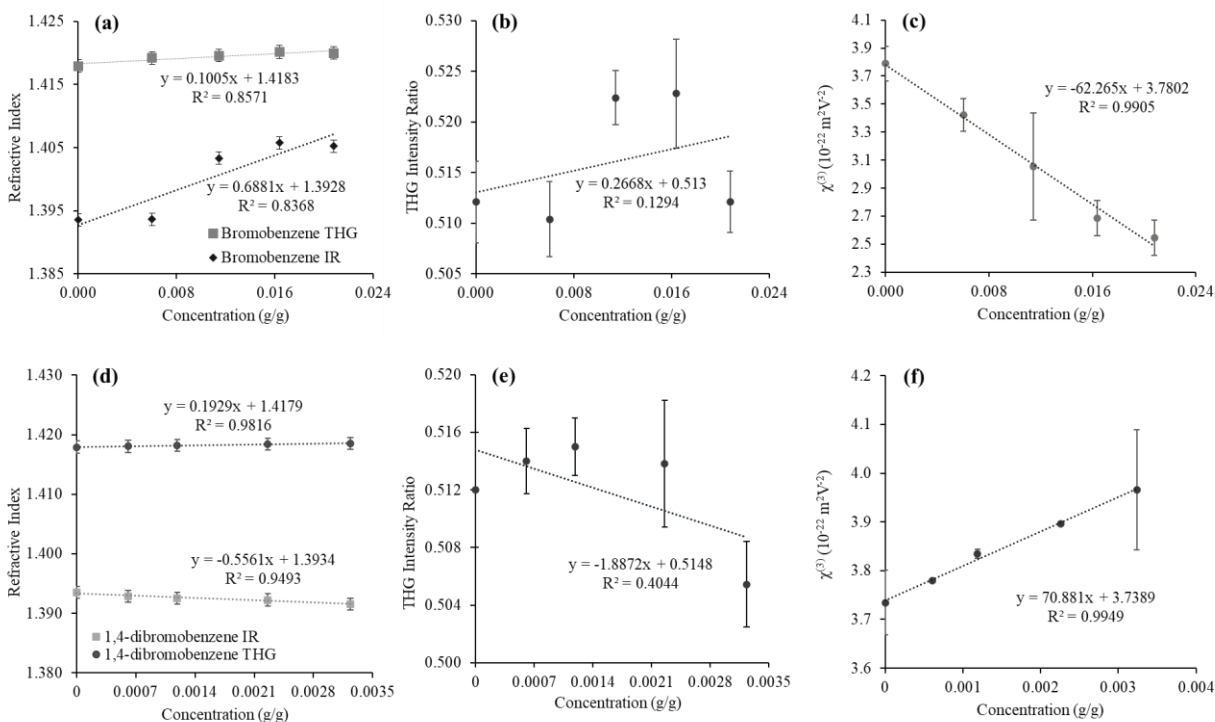
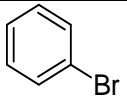
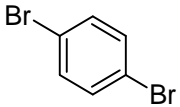
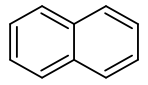
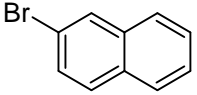
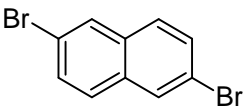
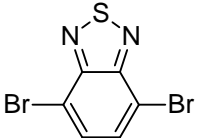
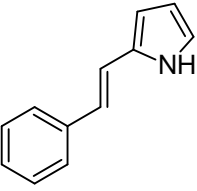
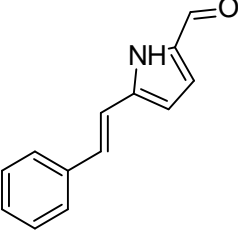


Figure 14. The refractive indices and THG intensity ratios used in the determination of the second hyperpolarizability value for bromobenzene and 1,4-dibromobenzene. The refractive indices taken at 343 nm (THG) and 1030 nm (IR) for bromobenzene (a) and 1,4-dibromobenzene (d), the THG intensity ratios for bromobenzene (b) and 1,4-dibromobenzene (e), and the third order nonlinear susceptibility values plotted over the concentration of the diluted bromobenzene solutions (c) and 1,4-dibromobenzene solutions (f).

The larger γ value observed for the compound compared to the solvent is likely due to bromobenzene's aromaticity. This result agrees with what was reported by Chen *et al.*, where compounds with higher levels of aromaticity were observed to have larger γ values.²⁴ Additionally, the dipole moment for bromobenzene is higher than that of THF which could be contributing to the difference observed between their γ values. This relationship between dipole moment and γ values has been reported previously.⁴⁰

Following this, the γ value of 1,4-dibromobenzene was calculated to be $103 \pm 7 \times 10^{-44} \text{ m}^2\text{V}^{-2}$ and the γ value for the solvent was calculated to be $1.7 \pm 0.1 \times 10^{-44} \text{ m}^2\text{V}^{-2}$ (Table 2). Similar to bromobenzene, the THG intensity ratios only appear to have a small deviation from the value observed for the solvent (Figure 14e). This indicates that the refractive indices are the major contributor to the γ value. The γ value for 1,4-dibromobenzene is positive indicating that it is in phase with the solvent. It is also around twice the magnitude of the γ value observed for bromobenzene. The presence of the additional bromine atom could be contributing to the increase observed for the γ value. This is supported by what was reported by Aguiar *et al.*, where there was an increase observed in the γ value for 2,3-dimethoxybenzaldehyde when a bromine atom was introduced.³³ Additionally, the higher γ value may also be from the extension of the conjugated π -system by the additional bromine. The dipole moment of 1,4-dibromobenzene is lower than that of bromobenzene. This indicates that the extended conjugation of the π -system by the additional bromine may be a greater contributor to the THG signal generated by the molecule than the dipole moment of the compound.

Table 2. The structure and name of the compound and its experimental γ value.

Structure	Compound Name	γ value ($10^{-44} \text{ m}^2\text{V}^{-2}$)
	Bromobenzene	-60 ± 2
	1,4-dibromobenzene	103 ± 7
	Naphthalene	-70 ± 10
	2-bromonaphthalene	-900 ± 200
	2,6-dibromonaphthalene	90 ± 10
	4,7-dibromobenzo[c]-1,2,5-thiadiazole (DBTD)	-900 ± 200
	2-(2-phenylethenyl)-1H-pyrrole (AAA40)	-900 ± 100
	5-(2-Phenylethenyl)-1H-pyrrole-2-carboxaldehyde (AAA41)	-140 ± 20

4.2.2 Naphthalene Cores

A series of naphthalene compounds which were also used as base groups were measured; compounds in this series included naphthalene, 2-bromonaphthalene, and 2,6-dibromonaphthalene. Only 3 diluted solutions were used for the naphthalene measurement which differed from the rest of the series where 4 diluted solutions were prepared. The refractive indices at 343 nm (THG) and 1030 nm (IR) can be seen in Figure 15a and 16a,d. In Figure 15b and 16b,e the THG intensities for each compound are shown. The calculated $\chi^{(3)}$ values are shown in Figure 15c and 16c,f plotted against concentration, which was used to calculate γ .

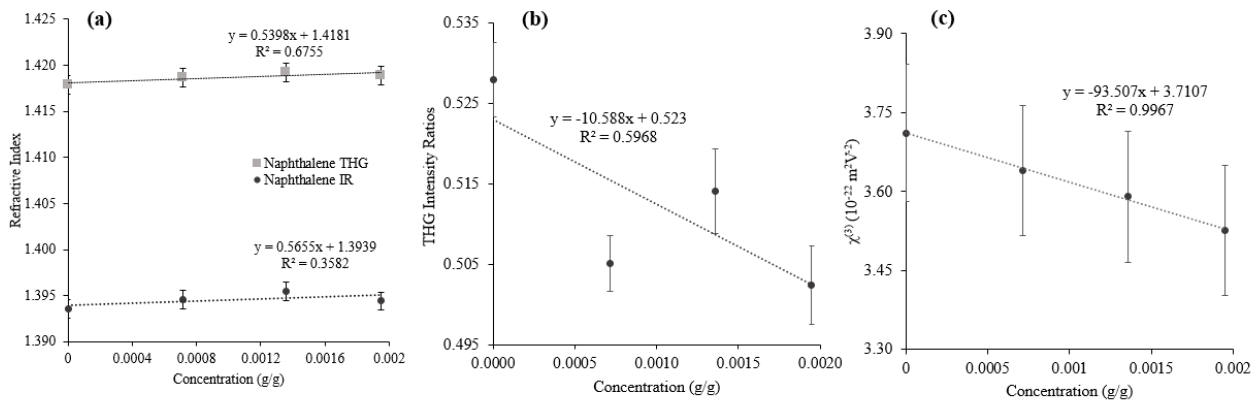


Figure 15. The refractive indices and THG intensity ratios used in the determination of the second hyperpolarizability value for naphthalene. The refractive indices taken at 343 nm (THG) and 1030 nm (IR) (a), the THG intensity ratios (b), and the third order nonlinear susceptibility values (c) plotted over the concentration of the naphthalene solutions.

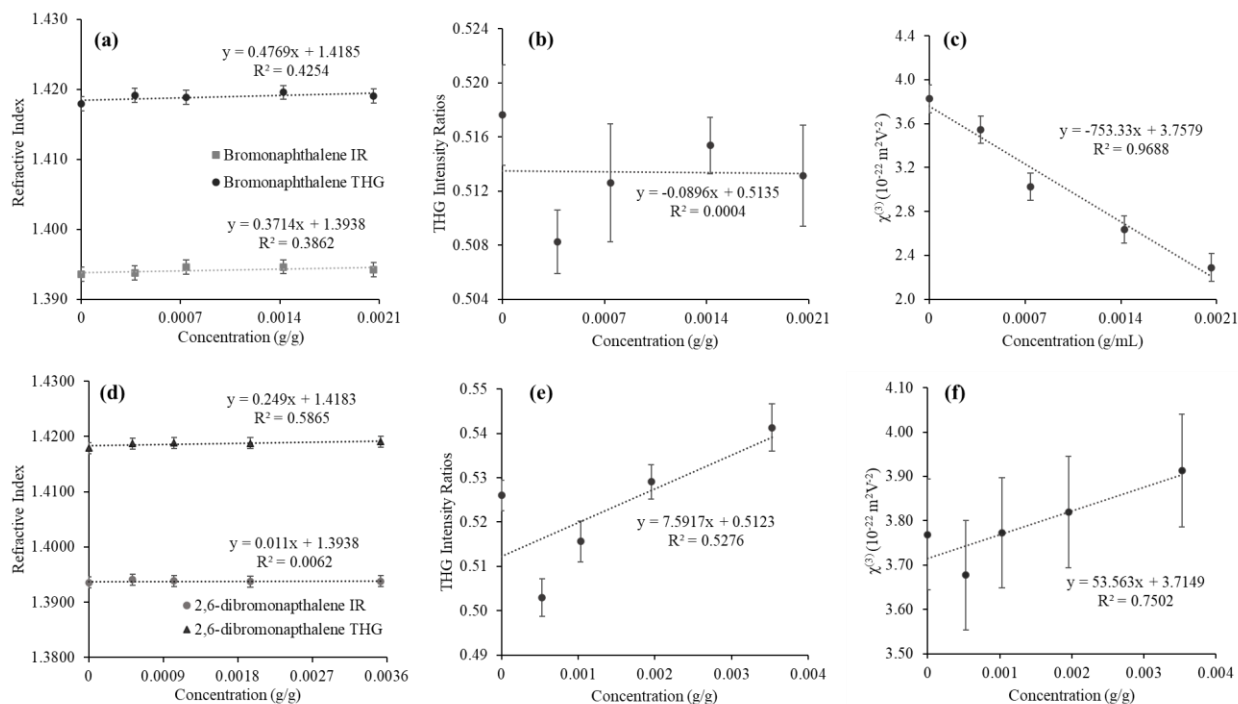


Figure 16. The refractive indices and THG intensity ratios used in the determination of the second hyperpolarizability value for 2-bromonaphthalene and 2,6-dibromonaphthalene. The refractive indices taken at 343 nm (THG) and 1030 nm (IR) 2-bromonaphthalene (a) and 2,6-dibromonaphthalene (d), the THG intensity ratios 2-bromonaphthalene (b) and 2,6-dibromonaphthalene (e), and the third order nonlinear susceptibility values plotted over the concentration of the 2-bromonaphthalene solutions (c) and 2,6-dibromonaphthalene solutions (f).

For naphthalene, the calculated γ value is $-70 \pm 10 \times 10^{-44} \text{ m}^2 \text{ V}^{-2}$ (Table 2) and the calculated γ value for the solvent is $1.6 \pm 0.2 \times 10^{-44} \text{ m}^2 \text{ V}^{-2}$. The γ value observed for naphthalene is $\sim 46 \times$ higher in magnitude than the γ value observed for the solvent. Additionally, naphthalene is out of phase with the solvent since a negative γ value is observed. The THG intensity ratio exhibits a larger change compared to what was observed for the benzene ring series. This change indicates that the THG intensity ratio contributes more to the calculated γ value observed for the compound than what was seen for the benzene ring series. The higher γ value observed for naphthalene compared

to the solvent, THF, can be attributed to the aromaticity of naphthalene. This would agree with what has been previously reported in the literature where aromaticity increases the γ value observed for compounds. Naphthalene also has a slightly higher γ value compared to bromobenzene. This can be attributed to the higher level of conjugation from the additional ring present in its structure. This agrees with Balu *et al.* where it was reported that the number of rings present in a compound had an influence on the γ value observed.²⁷ The dipole moment of naphthalene is lower than bromobenzene's dipole moment. This indicates that extended conjugation has a greater influence on the THG generated by a compound than dipole moment, which agrees with what was observed for 1,4-dibromobenzene.

Naphthalene's γ value has been previously reported in the literature, where it has been determined experimentally.⁴³ Bethea experimentally determined the γ value for naphthalene by measuring it as a liquid at 102°C.⁴³ The observed γ value was reported to be $8 \pm 2 \times 10^{-36}$ esu which is $11 \pm 2 \times 10^{-44} \text{ m}^2\text{V}^{-2}$.⁴³ This was converted following: $1 \text{ esu} = 1.398 \times 10^{-8} \text{ m}^2\text{V}^{-2}$ for $\chi^{(3)}$.⁴⁴ The γ value for naphthalene determined in this work is 7× higher than what was previously reported.⁴³ This difference may be from a difference in measurement conditions, where the naphthalene was previously measured at 102°C instead of 21°C.⁴³ Additionally, there may also be some error with the calculated γ value as less dilute solutions were prepared. Due to this, a series of 4 diluted solutions for naphthalene will be prepared to account for this potential error.

The γ value observed for 2-bromonaphthalene is $-900 \pm 200 \times 10^{-44} \text{ m}^2\text{V}^{-2}$ (Table 2), whereas the calculated γ value for the solvent is $1.6 \pm 0.2 \times 10^{-44} \text{ m}^2\text{V}^{-2}$. Since the γ value for 2-bromonaphthalene is negative, it is out of phase with the solvent. The γ value observed for 2-bromonaphthalene is ~13× higher in magnitude than the γ value observed for naphthalene. Unlike the THG intensity ratios observed for naphthalene, there was minimal change in the THG intensity

ratio values observed for 2-bromonaphthalene. This indicates that the refractive indices for the compound contribute more than the THG intensity ratios for the observed γ value. The difference in the γ value observed for 2-bromonaphthalene compared to naphthalene can be attributed to the addition of the bromine functional group. Aguiar *et al.* also observed larger γ values with the addition of a bromine functional group.³³ However, the difference in the γ value observed between 2-bromonaphthalene and naphthalene is higher than what was observed between bromobenzene and 1,4-dibromobenzene. This suggests that the addition of a bromine functional group to an unsubstituted compound has a greater effect on the THG generated from that compound than when the compound has already been substituted with a bromine.

Levine *et al.* experimentally determined the γ value for benzene, which they reported as $2.3 \pm 0.4 \times 10^{-36}$ esu or $3.3 \pm 0.5 \times 10^{-44} \text{ m}^2\text{V}^{-2}$.⁴⁵ The γ value of bromobenzene determined in this work is greater than what was previously reported for benzene by an order of magnitude. However, when comparing bromobenzene and 1,4-dibromobenzene less of an increase is observed. Notably the increase in γ between naphthalene and 2-bromonaphthalene is also an order of magnitude. This supports the suggestion that the addition of the first bromine functional group has a greater effect on the THG signal generated by the compound than the addition of a second bromine.

The calculated γ value of 2,6-dibromonaphthalene is $90 \pm 10 \times 10^{-44} \text{ m}^2\text{V}^{-2}$ (Table 2) and the γ value for the solvent is $1.6 \pm 0.1 \times 10^{-44} \text{ m}^2\text{V}^{-2}$. The observed γ value for 2,6-dibromonaphthalene is in phase with the solvent. The γ value of 2,6-dibromonaphthalene is also $10\times$ lower in magnitude than what was observed for 2-bromonaphthalene and comparable in magnitude to naphthalene's γ value. This observation indicates that the addition of a bromine functional group does not always result in an increase in the THG generated by the compound; this appears to contradict the results found for bromobenzene and 1,4-dibromobenzene, where the γ value increased slightly.

The molecular electrostatic potential plots (MEP) are shown in Figure 17 for naphthalene (a) and 2,6-dibromonaphthalene (b).^{46,47} The regions on the plots which are coloured red are negatively charged and have the highest electron density. The blue regions are positively charged and have lowest electron density. Based on Figure 17c and d, the MEPs of both naphthalene and 2,6-dibromonaphthalene appear to have similar electron distributions.^{46,47} In both, the highest electron density is seen in the region where the benzene rings fuse. One possible reason for why this is observed in 2,6-dibromonaphthalene is due to the electron donating nature of the bromine substituents. Since the compound is symmetrically substituted, the bromine functional groups are donating their electrons into the ring system and no dipole moment is observed. The similarity between naphthalene and 2,6-dibromonaphthalene electron density distribution could be a contributing factor for why their γ values are comparable in magnitude. Since the 2-bromonaphthalene is not symmetrically substituted it has a non-zero dipole moment present in the molecule. The combination of the dipole moment and the increased conjugation from the additional ring may be contributing to the much larger γ value observed for 2-bromonaphthalene compared to the naphthalene and 2,6-dibromonaphthalene. This is supported by the results reported in Sofiani *et al.*, where the presence of a dipole moment was observed to increase the THG generated by the compound.⁴⁰

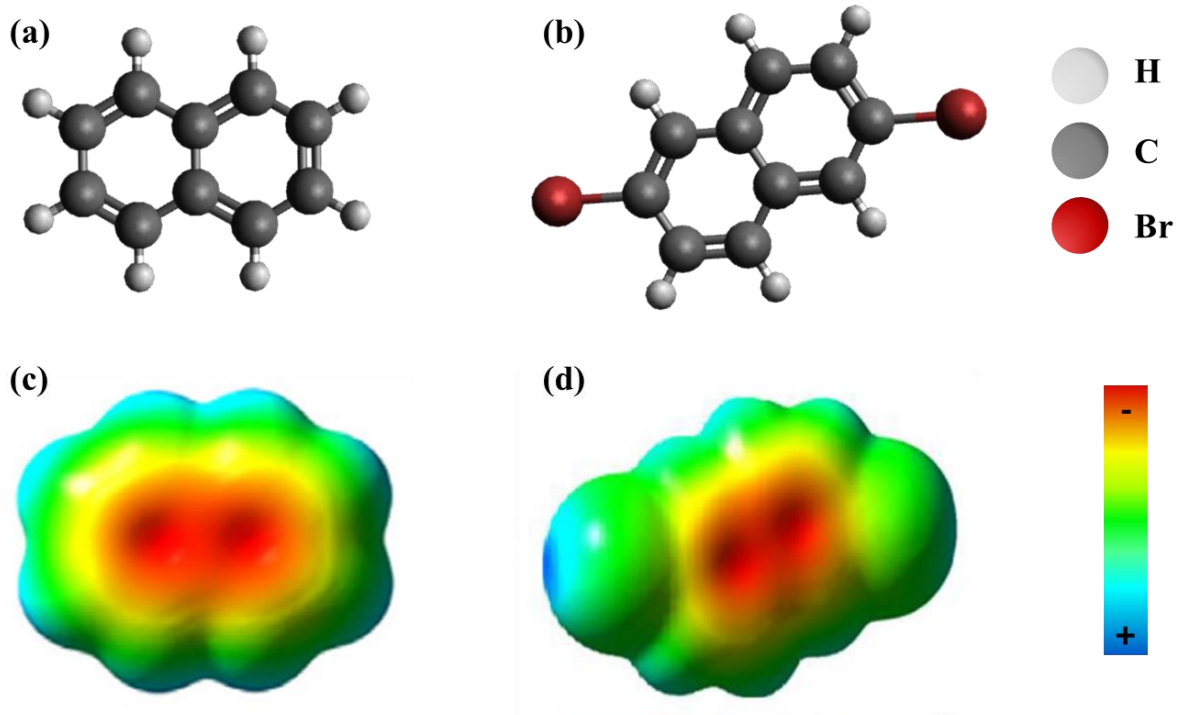


Figure 17. Pictorial representation of naphthalene (a) and 2,6-dibromonaphthalene (b) molecular structures. The MEP for naphthalene (c) (Reproduced with permission from Spectrochimica acta part A: molecular and biomolecule spectroscopy, Elsevier)⁴⁷ and 2,6-dibromonaphthalene (d) (Reproduced with permission from Journal of Molecular Structure, Elsevier)⁴⁶. Red regions are negatively charged whereas blue regions are positively charged.

4.2.3 4,7-dibromobenzo[*c*]-1,2,5-thiadiazole

Following the 1,4-bromobenzene solutions, the refractive indices (Figure 18a) and THG intensity ratios (Figure 18b) for 4,7-dibromobenzo[*c*]-1,2,5-thiadiazole (DBTD) solutions were measured. The $\chi^{(3)}$ values (Figure 18c) were then calculated and used to calculate the γ values.

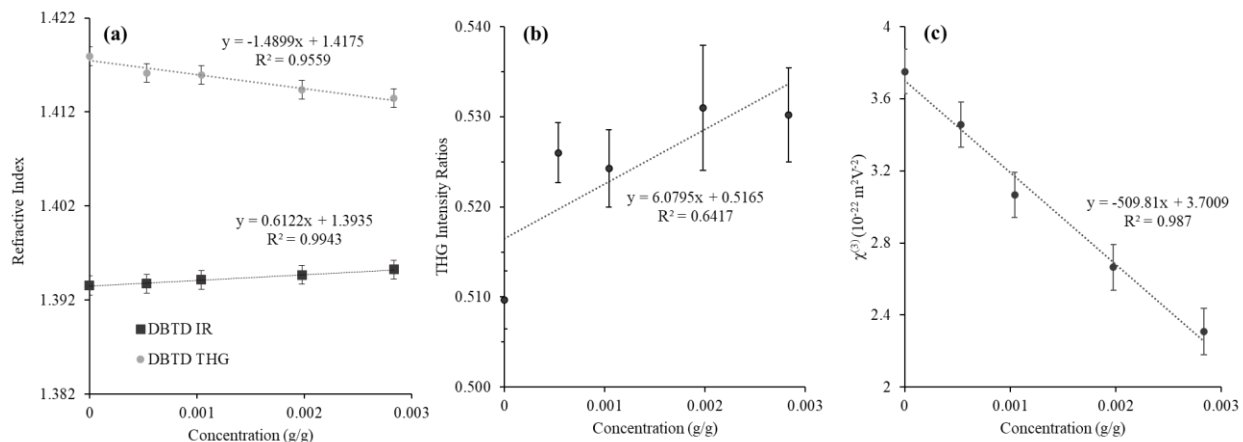


Figure 18. The refractive indices and THG intensity ratios used in the determination of the second hyperpolarizability value for DBTD. The refractive indices taken at 343 nm (THG) and 1030 nm (IR) (a), the THG intensity ratios (b), and the third order nonlinear susceptibility values (c) plotted over the concentration of the DBTD diluted solutions.

The γ value of the solvent was $1.8 \pm 0.5 \times 10^{-44} \text{ m}^2 \text{ V}^{-2}$, and the γ value for 4,7-dibromobenzo[c]-1,2,5-thiadiazole (DBTD) was $-900 \pm 200 \times 10^{-44} \text{ m}^2 \text{ V}^{-2}$ (Table 2). For DBTD the observed γ value is similar to what was determined for 2-bromonaphthalene. The γ value is $\sim 9 \times$ greater in magnitude than 1,4-bromobenzene and an order of magnitude larger than bromobenzene. The γ value may be higher due to the increase in electron density from the addition of the 1,2,5-thiadiazole ring. This addition also increases the conjugation which also could contribute to the larger γ observed. This would agree with Balu *et al.* and Motomura *et al.* who have both reported that increases in conjugation are associated with larger γ values.^{27,37}

4.3 Pyrrole Compounds for Potential Dye Complexes

4.3.3 2-(2-phenylethenyl)-1H-pyrrole (AAA40)

The compound referred to as AAA40 is derived from the bromobenzene starting material. The refractive indices (Figure 19a) and THG intensity ratios (Figure 19b) for the AAA40 solutions were measured. The $\chi^{(3)}$ values (Figure 19c) were then calculated and used to calculate the γ values.

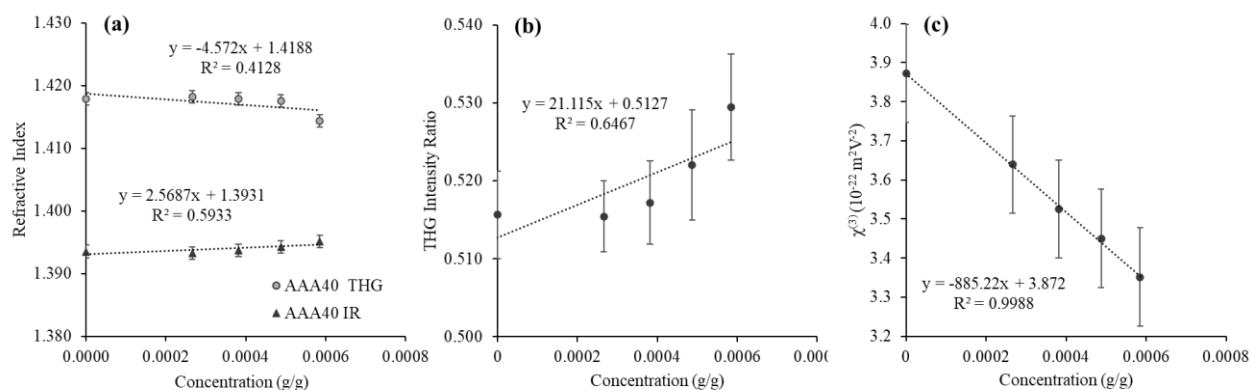


Figure 19. The refractive indices and THG intensity ratios used in the determination of the second hyperpolarizability value for AAA40. The refractive indices taken at 343 nm (THG) and 1030 nm (IR) (a), the THG intensity ratios (b), and the third order nonlinear susceptibility values (c) plotted over the concentration of the AAA40 diluted solutions.

The calculated γ value for the solvent was $1.7 \pm 0.2 \times 10^{-44} \text{ m}^2 \text{ V}^{-2}$ and the γ value for AAA40 was $-900 \pm 100 \text{ m}^2 \text{ V}^{-2}$ (Table 2). The value is negative indicating that the compound is in opposite phase of the solvent. When compared to the bromobenzene starting material the γ value has increased by an order of magnitude. The increase of conjugation observed from the addition of the pyrrole substituent may be a contributing factor as to why the γ value is larger. This observation is supported by Balu *et al.* and Motomura *et al.* who reported that increased conjugation is associated with larger γ values.^{27,37} The γ value observed for AAA40 is similar to the γ value observed for the 2-bromonaphthalene and 4,7-dibromobenzo[c]-1,2,5-thiadiazole. Notably, this is

8× lower in magnitude than the γ value observed for β -carotene.³ This indicates that the pyrrole compound would need further derivatization in order to be useful as a dye for THG microscopy.

4.3.4 5-(2-Phenylethenyl)-1H-pyrrole-2-carboxaldehyde (AAA41)

The compound referred to as AAA41 is derived from the bromobenzene starting material. The refractive indices (Figure 20a) and THG intensity ratios (Figure 20b) for the AAA41 solutions were measured. The $\chi^{(3)}$ values (Figure 20c) were then determined and used to calculate the γ value.

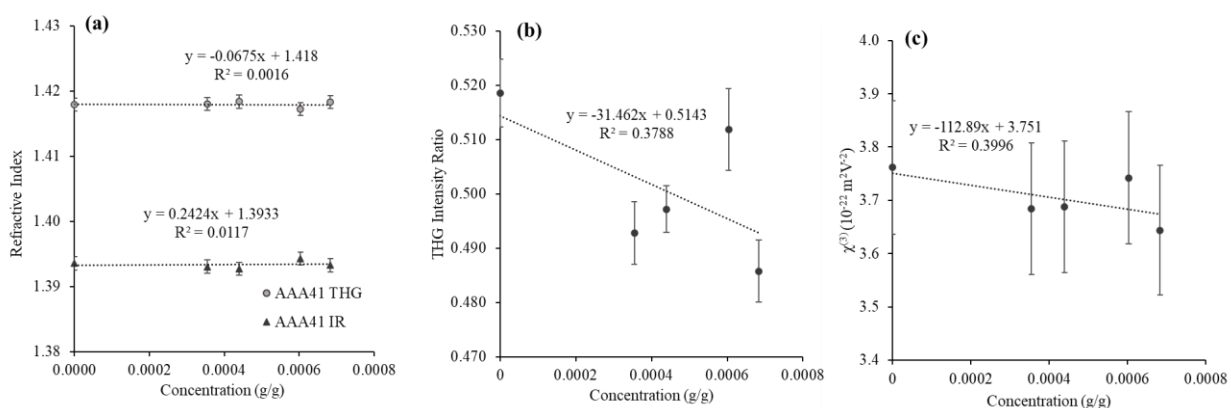


Figure 20. The refractive indices and THG intensity ratios used in the determination of the second hyperpolarizability value for AAA41. The refractive indices taken at 343 nm (THG) and 1030 nm (IR) (a), the THG intensity ratios (b), and the third order nonlinear susceptibility values (c) plotted over the concentration of the AAA41.

The calculated γ value for the solvent was $1.7 \pm 0.1 \times 10^{-44} \text{ m}^2\text{V}^{-2}$ and the γ value for AAA41 was $-140 \pm 20 \times 10^{-44} \text{ m}^2\text{V}^{-2}$ (Table 2). The value is negative indicating that the compound is out of phase with the solvent. When compared to the starting material, bromobenzene, the γ value is 2× higher in magnitude. This indicates that the addition of the pyrrole-2-carboxaldehyde group results in a higher increase in γ compared to the bromine functional group. However, the γ value is 9× lower in magnitude than what was observed for AAA40. This is despite the addition of the pyrrole-

2-carboxaldehyde group increasing the conjugation of compound and having a stronger dipole moment than AAA40. In this, the result disagrees with the findings from Balu *et al.* and Motomura *et al.* where increasing a compounds conjugation was reported to lead to an increase in the γ value observed.^{27,37} It also disagrees with previous literature that associated having a stronger dipole moment with larger γ values.⁴⁰ One possible reason for this deviation is differences in the absorbance at either the 343 or 1030 nm wavelength, which could influence the results. Absorbance at the THG wavelength has been observed to effect the refractive indexes collected for the solutions; this in turn resulted in a change in the γ value.³ Further work on investigating the difference between the two pyrrole compounds includes collection and comparison of UV-vis spectra.

Chapter 5: CONCLUSION

In this work, initial studies on salt solutions were performed to determine the γ value for NaCl and MgSO₄. For NaCl, γ value was determined to be $1.7 \pm 0.2 \times 10^{-44} \text{ m}^2 \text{V}^{-2}$, this agreed with previous literature results where the γ value was reported as $2.1 \pm 0.5 \times 10^{-44} \text{ m}^2 \text{V}^{-2}$.⁸ The γ value for MgSO₄ could not be calculated due to a change in slope observed for both the THG ratio intensity and the χ^3 graphs. This change was attributed to the concentration-dependent transition in the solvent shell of MgSO₄, which has been reported in the literature.⁴²

The γ values for several starting material core compounds with differing levels of substitution were determined and compared. Benzene ring core starting materials included bromobenzene and 1,4-dibromobenzene. The γ value for 1,4-bromobenzene was determined to be the largest for the series, this was attributed to the addition of the bromine functional groups. Naphthalene core starting materials included: naphthalene, 2-bromonaphthalene, and 2,6-dibromonaphthalene. Unlike with the benzene core series, the less substituted naphthalene, 2-bromonaphthalene, had the largest γ value. The 2,6-dibromonaphthalene had a smaller γ value than 2-bromonaphthalene and was similar to naphthalene. This was attributed to the similarity between electron density distribution seen between 2,6-dibromonaphthalene and naphthalene. 4,7-dibromobenzo[c]-1,2,5-thiadiazole (DBTD) was also evaluated as a core starting material. The observed γ value for DBTD was similar to 2-dibromonaphthalene and larger than all the other starting material core compounds.

The γ values of pyrrole compounds associated with the bromobenzene starting materials were determined and compared. AAA40 was found to have a higher γ value than AAA41. This was unexpected as it disagreed with previous findings which would suggest that a larger γ value

should be observed for AAA41 due to its increased level of conjugation and larger dipole moment.

27,37,36

When comparing the γ values of the compounds to the γ value to β -carotene, the closest were AAA40, 2-bromonaphthalene, and DBTD, where they all were within the $900 \times 10^{-44} \text{ m}^2\text{V}^{-2}$ range. This is still $8 \times$ lower than the γ value observed for β -carotene.³ For AAA40, this indicates that further derivatization in order to be useful as a dye for THG microscopy. With 2-bromonaphthalene and DBTD, this indicates that they are promising starting material for dyes to be built around as they already generate strong THG signal.

Chapter 6: FUTURE WORK

Further steps for this project include measuring and calculating the γ values for the remaining pyrrole compounds and ruthenium complexes. The results collected for the starting material cores from this project will be used to assess the ability to predict the relative γ values associated with the metal complexes. This will provide insight into ways to optimize the metal complexes so that they can act as strong harmonophores and good candidates for dyes for THG microscopy. The naphthalene series will also be remeasured using a set of 4 dilute solutions. UV-vis spectroscopy will be used to determine if absorbance is occurring in the 1030 or 343 nm range for all compounds as absorbance may be interfering with the results observed.

A computational study into the γ values of the starting material cores will be done using Time-Dependent Hartree-Fock (TDHF). Calculating the γ values computationally will provide an advantage over the experimentally determined γ values as the calculations are performed in vacuum and are not influenced by a solvent. This allows for the γ values of the compounds to be compared with those that are not soluble in THF. It is also valuable because these compounds will not be used in THF if they are explored further for applications as dyes. Lastly, an exploratory study will be conducted on various salt solutions to assess the influence that solvent-ion interactions have on the THG intensity ratios.

CHAPTER 7: REFERENCES

- (1) Dietzel, S. Third Harmonic Generation Microscopy. *Wiley Analytical Science*. November 2014. <https://analyticalscience.wiley.com/doi/10.1002/imaging.4877/>.
- (2) Sun, C. K. Higher Harmonic Generation Microscopy. *Adv Biochem Eng Biotechnol* **2005**, *95*, 17–56. <https://doi.org/10.1007/b102209>.
- (3) Tokarz, D.; Cisek, R.; Garbaczewska, M.; Sandkuijl, D.; Qiu, X.; Stewart, B.; Levine, J. D.; Fekl, U.; Barzda, V. Carotenoid Based Bio-Compatible Labels for Third Harmonic Generation Microscopy. *Physical Chemistry Chemical Physics* **2012**, *14* (30), 10653–10661. <https://doi.org/10.1039/c2cp41583f>.
- (4) Tokarz, D.; Cisek, R.; Fekl, U.; Barzda, V. The Molecular Second Hyperpolarizability of the Light-Harvesting Chlorophyll a/b Pigment-Protein Complex of Photosystem II. *Journal of Physical Chemistry B* **2013**, *117* (38), 11069–11075. <https://doi.org/10.1021/jp400739v>.
- (5) Purvis, K.; Brittain, K.; Joseph, A.; Cisek, R.; Tokarz, D. Third-Order Nonlinear Optical Properties of Phycobiliproteins from Cyanobacteria and Red Algae. *Chem Phys Lett* **2019**, *731* (July), 136599. <https://doi.org/10.1016/j.cplett.2019.136599>.
- (6) Boyd, R. W. *Nonlinear Optics*, 3rd ed.; Academic press, 2008.
- (7) Stucky, G. D.; Marder, S. R.; Sohn, J. E. Linear and Nonlinear Polarizability. **1991**, 2–30. <https://doi.org/10.1021/bk-1991-0455.ch001>.
- (8) Tokarz, D.; Cisek, R.; Prent, N.; Fekl, U.; Barzda, V. Measuring the Molecular Second Hyperpolarizability in Absorptive Solutions by the Third Harmonic Generation Ratio Technique. *Anal Chim Acta* **2012**, *755*, 86–92. <https://doi.org/10.1016/j.aca.2012.09.049>.
- (9) Sakki, B.; Taboukhat, S.; Messaadia, L.; Guergouri, M.; Bouraiou, A.; Nasri, R.; Figa, V.; Bouchouit, K.; Sahraoui, B. DFT Analysis and Third-Harmonic Generation Properties of One Series of Push–Pull Benzylidenemalononitrile Derivatives. *European Physical Journal D* **2022**, *76* (6), 1–11. <https://doi.org/10.1140/epjd/s10053-022-00424-4>.
- (10) Tuer, A. E.; Krouglov, S.; Prent, N.; Cisek, R.; Sandkuijl, D.; Yasufuku, K.; Wilson, B. C.; Barzda, V. Nonlinear Optical Properties of Type i Collagen Fibers Studied by Polarization

- Dependent Second Harmonic Generation Microscopy. *Journal of Physical Chemistry B* **2011**, *115* (44), 12759–12769. <https://doi.org/10.1021/jp206308k>.
- (11) Golaraei, A.; Mirsanaye, K.; Ro, Y.; Krouglov, S.; Akens, M. K.; Wilson, B. C.; Barzda, V. Collagen Chirality and Three-Dimensional Orientation Studied with Polarimetric Second-Harmonic Generation Microscopy. *J Biophotonics* **2019**, *12* (1), 1–9. <https://doi.org/10.1002/jbio.201800241>.
- (12) Campbell, K. R.; Campagnola, P. J.; Campbell, K. R.; Chaudhary, R.; Handel, J. M.; Patankar, M. S.; Campagnola, P. J. Polarization-Resolved Second Harmonic Generation Imaging of Human Ovarian Cancer. *J Biomed Opt* **2018**, *23* (06), 1. <https://doi.org/10.1117/1.jbo.23.6.066501>.
- (13) Cisek, R.; Tokarz, D.; Krouglov, S.; Steup, M.; Emes, M. J.; Tetlow, I. J.; Barzda, V. Second Harmonic Generation Mediated by Aligned Water in Starch Granules. *Journal of Physical Chemistry B* **2014**, *118* (51), 14785–14794. <https://doi.org/10.1021/jp508751s>.
- (14) Cisek, R.; Tokarz, D.; Krouglov, S.; Steup, M.; Emes, M. J.; Tetlow, I. J.; Barzda, V. Second Harmonic Generation Mediated by Aligned Water in Starch Granules. *Journal of Physical Chemistry B* **2014**, *118* (51), 14785–14794. <https://doi.org/10.1021/jp508751s>.
- (15) Santos, E. M.; Sheng, W.; Esmatpour Salmani, R.; Tahmasebi Nick, S.; Ghanbarpour, A.; Gholami, H.; Vasileiou, C.; Geiger, J. H.; Borhan, B. Design of Large Stokes Shift Fluorescent Proteins Based on Excited State Proton Transfer of an Engineered Photobase. *J Am Chem Soc* **2021**, *143* (37), 15091–15102. <https://doi.org/10.1021/jacs.1c05039>.
- (16) Ramos-Ortiz, G.; Maldonado, J. L.; Meneses-Nava, M. A.; Barbosa-García, O.; Olmos, M.; Cha, M. Third-Harmonic Generation Performance of Organic Polymer Films Doped with Triphenylmethane Derivative Dyes. *Opt Mater (Amst)* **2007**, *29* (6), 636–641. <https://doi.org/10.1016/j.optmat.2005.11.010>.
- (17) Liu, M.; Quah, H. S.; Wen, S.; Yu, Z.; Vittal, J. J.; Ji, W. Efficient Third Harmonic Generation in a Metal-Organic Framework. *Chemistry of Materials* **2016**, *28* (10), 3385–3390. <https://doi.org/10.1021/acs.chemmater.6b00632>.

- (18) Carriles, R.; Schafer, D. N.; Sheetz, K. E.; Field, J. J.; Cisek, R.; Barzda, V.; Sylvester, A. W.; Squier, J. A. Invited Review Article: Imaging Techniques for Harmonic and Multiphoton Absorption Fluorescence Microscopy. *Review of Scientific Instruments* **2009**, *80* (8), 1–23. <https://doi.org/10.1063/1.3184828>.
- (19) Shcheslavskiy, V.; Petrov, G.; Yakovlev, V. V. Nonlinear Optical Susceptibility Measurements of Solutions Using Third-Harmonic Generation on the Interface. *Appl Phys Lett* **2003**, *82* (22), 3982–3984. <https://doi.org/10.1063/1.1579866>.
- (20) Kajzar, F.; Ledoux, I.; Zyss, J. Electric-Field-Induced Optical Second-Harmonic Generation in Polydiacetylene Solutions. *Phys Rev A (Coll Park)* **1987**, *36* (5), 2210–2219. <https://doi.org/10.1103/PhysRevA.36.2210>.
- (21) Bhattacharya, J. C. Refractive Index Measurement. *Opt Laser Technol* **1987**, *19* (1), 29–32. [https://doi.org/10.1016/0030-3992\(87\)90008-9](https://doi.org/10.1016/0030-3992(87)90008-9).
- (22) Gavgiotaki, E.; Filippidis, G.; Markomanolaki, H.; Kenanakis, G.; Agelaki, S.; Georgoulas, V.; Athanassakis, I. Distinction between Breast Cancer Cell Subtypes Using Third Harmonic Generation Microscopy. *J Biophotonics* **2017**, *10* (9), 1152–1162. <https://doi.org/10.1002/jbio.201600173>.
- (23) Kuzmin, N. V.; Wesseling, P.; Hamer, P. C. de W.; Noske, D. P.; Galgano, G. D.; Mansvelder, H. D.; Baayen, J. C.; Groot, M. L. Third Harmonic Generation Imaging for Fast, Label-Free Pathology of Human Brain Tumors. *Biomed Opt Express* **2016**, *7* (5), 1889. <https://doi.org/10.1364/boe.7.001889>.
- (24) Chen, J.; Zhu, X.; Luo, C.; Dai, Y. Electronic and Optical Properties of Pyrrole and Thiophene Oligomers: A Density Functional Theory Study. *Int J Quantum Chem* **2017**, *117* (24), 1–9. <https://doi.org/10.1002/qua.25453>.
- (25) Mydlova, L.; Taboukhat, S.; Ayadi, A.; Migalska-Zalas, A.; El-Ghayoury, A.; Zawadzka, A.; Makowska-Janusik, M.; Sahraoui, B. Theoretical and Experimental Investigation of Multifunctional Highly Conjugated Organic Push-Pull Ligands for NLO Applications. *Opt Mater (Amst)* **2018**, *86* (October), 304–310. <https://doi.org/10.1016/j.optmat.2018.10.017>.

- (26) Reinhardt, B. A.; Unroe, M. R.; Evers, R. C.; Zhao, M.; Samoc, M.; Prasad, P. N.; Sinsky, M. Third-Order Optical Nonlinearities of Model Compounds Containing Benzobisthiazole, Benzobisoxazole, and Benzbisimidazole Units. *Chemistry of Materials* **1991**, *3* (5), 864–871. <https://doi.org/10.1021/cm00017a023>.
- (27) Balu, R.; Korambath, P.; Pandey, R.; Karna, S. P. Ab Initio Study of Nonlinear Optical Properties of Aromatic Fused Rings. *Chem Phys Lett* **2013**, *590*, 58–62. <https://doi.org/10.1016/j.cplett.2013.10.078>.
- (28) Tokarz, D.; Tuer, A.; Cisek, R.; Krouglov, S.; Barzda, V. Ab Initio Calculations of the Linear and Nonlinear Optical Properties of Amino Acids. *J Phys Conf Ser* **2010**, *256* (1). <https://doi.org/10.1088/1742-6596/256/1/012015>.
- (29) Librando, V.; Alparone, A.; Minniti, Z. Computational Study on Dipole Moment, Polarizability and Second Hyperpolarizability of Nitronaphthalenes. *Journal of Molecular Structure: THEOCHEM* **2008**, *856* (1–3), 105–111. <https://doi.org/10.1016/j.theochem.2008.01.022>.
- (30) Sahki, F. A.; Bouraiou, A.; Taboukhat, S.; Messaadia, L.; Bouacida, S.; Figa, V.; Bouchouit, K.; Sahraoui, B. Design and Synthesis of Highly Conjugated Electronic Phenanthrolines Derivatives for Remarkable NLO Properties and DFT Analysis. *Optik (Stuttg)* **2021**, *241* (March), 166949. <https://doi.org/10.1016/j.ijleo.2021.166949>.
- (31) Sun, L.; Wang, S. Slow-Accumulated Optical Nonlinearity in Chlorophyll a Solution. *4268* (2001), 88–96.
- (32) Maldonado, J. L.; Rodríguez, M. Organic Non-Linear Optics and Opto-Electronics. *Condens Matter Phys* **2010**, 117–126.
- (33) Aguiar, A. S. N.; dos Santos, V. D.; Borges, I. D.; Navarrete, A.; Aguirre, G.; Valverde, C.; Camargo, A. J.; Oliveira, S. S.; Osório, F. A. P.; Fonseca, T. L.; Napolitano, H. B. Bromine Substitution Effect on Structure, Reactivity, and Linear and Third-Order Nonlinear Optical Properties of 2,3-Dimethoxybenzaldehyde. *Journal of Physical Chemistry A* **2022**, *126* (43), 7852–7863. <https://doi.org/10.1021/acs.jpca.2c04658>.

- (34) Matsuzawa, N.; Dixon, D. A. Semiempirical Calculations of the Polarizability and Second-Order Hyperpolarizability of C₆₀, C₇₀, and Model Aromatic Compounds. *Journal of Physical Chemistry* **1992**, *96* (15), 6241–6247. <https://doi.org/10.1021/j100194a028>.
- (35) Electronic, I.; Contributions, V. Hyperpolarizabilities of Push – Pull Chromophores in Solution : **2022**.
- (36) Hermann, J. P.; Ducuing, J. Third-Order Polarizabilities of Long-Chain Molecules. *J Appl Phys* **1974**, *45* (11), 5100–5102. <https://doi.org/10.1063/1.1663197>.
- (37) Motomura, S.; Nakano, M.; Fukui, H.; Yoneda, K.; Kubo, T.; Carion, R.; Champagne, B. Size Dependences of the Diradical Character and the Second Hyperpolarizabilities in Dicyclopenta-Fused Acenes: Relationships with Their Aromaticity/Antiaromaticity. *Physical Chemistry Chemical Physics* **2011**, *13* (46), 20575–20583. <https://doi.org/10.1039/c1cp20773c>.
- (38) Papagiannouli, I.; Szukalski, A.; Iliopoulos, K.; Mysliwiec, J.; Couris, S.; Sahraoui, B. Pyrazoline Derivatives with a Tailored Third Order Nonlinear Optical Response. *RSC Adv* **2015**, *5* (60), 48363–48367. <https://doi.org/10.1039/c5ra05912g>.
- (39) Keshari, V.; Wijekoon, W. M. K. P.; Prasad, P. N.; Karna, S. P. Hyperpolarizabilities of Organic Molecules: Ab Initio Time-Dependent Coupled Perturbed Hartree - Fock - Roothaan Studies of Basic Heterocyclic Structures. *Journal of Physical Chemistry* **1995**, *99* (22), 9045–9050. <https://doi.org/10.1021/j100022a015>.
- (40) Sofiani, Z.; Khannyra, S.; Boucetta, A.; ElJouad, M.; Bouchouit, K.; Serrar, H.; Boukhris, S.; Souizi, A.; Migalska-Zalas, A. Nonlinear Optical Properties of New Synthesized Conjugated Organic Molecules Based on Pyrimidine and Oxazepine. *Opt Quantum Electron* **2016**, *48* (5), 1–12. <https://doi.org/10.1007/s11082-016-0549-3>.
- (41) Fernández, M.; Klapp, J.; Sigalotti, L. D. G.; Ruetter, F. Hydration Study of MgSO₄ Using Different Theoretical and Model Approaches. ¿is There a Proton Transfer? *Chem Phys Lett* **2018**, *713* (October), 39–45. <https://doi.org/10.1016/j.cplett.2018.10.018>.

- (42) Buchner, R.; Chen, T.; Hefter, G. Complexity in “Simple” Electrolyte Solutions: Ion Pairing in MgSO₄(Aq). *Journal of Physical Chemistry B* **2004**, *108* (7), 2365–2375. <https://doi.org/10.1021/jp034870p>.
- (43) Bethea, C. G. Measurement of Hyperpolarizabilities of Several Organic Molecules. *J Chem Phys* **1978**, *69* (3), 1312–1313. <https://doi.org/10.1063/1.436671>.
- (44) Shiri, D. Ab Initio Study of Nonlinear Optical Susceptibilities in Silicon Nanowires. *ArXiv* **2017**.
- (45) Levine, B. F.; Bethea, C. G. Second and Third Order Hyperpolarizabilities of Organic Molecules. *J Chem Phys* **1975**, *63* (6), 2666–2682. <https://doi.org/10.1063/1.431660>.
- (46) Sertbakan, T. R.; Özçelik, F. Molecular Structure, Quantum Chemical and Spectroscopic Properties of 2,6–Dibromonaphthalene by Density Functional Theory Calculations. *J Mol Struct* **2022**, *1250*. <https://doi.org/10.1016/j.molstruc.2021.131834>.
- (47) Amalanathan, M.; Joe, I. H.; Rastogi, V. K. Molecular Structure and Vibrational Spectral Investigation of Charge Transfer NLO Crystal Naphthalene Picrate for THz Application. *Spectrochim Acta A Mol Biomol Spectrosc* **2013**, *108*, 256–267. <https://doi.org/10.1016/j.saa.2013.01.097>.

CHAPTER 8: APPENDIX



Molecular structure and vibrational spectral investigation of charge transfer NLO crystal Naphthalene Picrate for THz application

Author: M. Amalanathan, I. Hubert Joe, V.K. Rastogi

Publication: Spectrochimica Acta Part A: Molecular and Biomolecular Spectroscopy

Publisher: Elsevier

Date: May 2013

Copyright © 2013 Elsevier B.V. All rights reserved.

Order Completed

Thank you for your order.

This Agreement between Ms. Elisha Bennett ("You") and Elsevier ("Elsevier") consists of your license details and the terms and conditions provided by Elsevier and Copyright Clearance Center.

Your confirmation email will contain your order number for future reference.

License Number 5515090919355

[Printable Details](#)

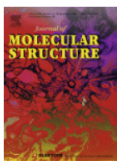
License date Mar 23, 2023

Licensed Content

Licensed Content Publisher	Elsevier
Licensed Content Publication	Spectrochimica Acta Part A: Molecular and Biomolecular Spectroscopy
Licensed Content Title	Molecular structure and vibrational spectral investigation of charge transfer NLO crystal Naphthalene Picrate for THz application
Licensed Content Author	M. Amalanathan, I. Hubert Joe, V.K. Rastogi
Licensed Content Date	May 1, 2013
Licensed Content Volume	108
Licensed Content Issue	n/a
Licensed Content Pages	12

Order Details

Type of Use	reuse in a thesis/dissertation
Portion	figures/tables/illustrations
Number of figures/tables/illustrations	1
Format	electronic
Are you the author of this Elsevier article?	No
Will you be translating?	No



Molecular structure, quantum chemical and spectroscopic properties of 2,6-dibromonaphthalene by density functional theory calculations

Author: Tevfik Raci Sertbakan, Fatmanur Özçelik

Publication: Journal of Molecular Structure

Publisher: Elsevier

Date: 15 February 2022

© 2021 Elsevier B.V. All rights reserved.

Order Completed

Thank you for your order.

This Agreement between Ms. Elisha Bennett ("You") and Elsevier ("Elsevier") consists of your license details and the terms and conditions provided by Elsevier and Copyright Clearance Center.

Your confirmation email will contain your order number for future reference.

License Number 5515091112539

[Printable Details](#)

License date Mar 23, 2023

Licensed Content

Licensed Content Publisher	Elsevier
Licensed Content Publication	Journal of Molecular Structure
Licensed Content Title	Molecular structure, quantum chemical and spectroscopic properties of 2,6-dibromonaphthalene by density functional theory calculations
Licensed Content Author	Tevfik Raci Sertbakan, Fatmanur Özçelik
Licensed Content Date	Feb 15, 2022
Licensed Content Volume	1250
Licensed Content Issue	n/a
Licensed Content Pages	1

Order Details

Type of Use	reuse in a thesis/dissertation
Portion	figures/tables/illustrations
Number of figures/tables/illustrations	1
Format	electronic
Are you the author of this Elsevier article?	No
Will you be translating?	No